

XP-12 Laser Interferometer

Table of Contents

1. FUNDAMENTALS	3
1.1 <i>Characteristics of light</i>	3
1.2 <i>Superimposition and Phase d</i>	6
1.3 <i>Interferometer</i>	6
1.4 <i>Real interferometer</i>	8
1.4.1 Contrast or visibility	8
1.4.2 Light sources and coherence	9
1.5 <i>Coherence</i>	9
1.6 <i>Thermal light</i>	9
1.7 <i>Cold light</i>	10
1.8 <i>Wave fronts</i>	13
1.9 <i>Gaussian beams</i>	14
1.10 <i>Technical interferometers</i>	15
1.10.1 Beam splitting prism	16
1.10.2 Triple reflector	17
1.10.3 Homodyne interferometer	17
1.10.4 Detection optics	18
1.10.5 Heterodyne interferometer	20
2. EXPERIMENTS	21
2.1 <i>Michelson Interferometer</i>	21
2.1.1 Adjustment of the Michelson Interferometer Step 1	23
2.1.2 Alignment Step 2	23
2.1.3 Step 3, alignment of the mirrors	24
2.1.4 Interference patterns	25
2.1.5 Measuring the contrast function $V(\delta L)$	25
2.2 <i>Technical interferometer</i>	26
2.2.1 Set-up of Technical Interferometer step 1	28
2.2.2 Set-up of the beam splitting and recombining module	28
2.2.3 Set-up of triple reflector TR1 and TR2	29
2.2.4 Set-up of the signal detection unit	30
2.2.5 Signal detection	30
2.2.6 Length measurement	31
2.3 <i>Set-up for CNC calibration</i>	31
2.3.1 Set-up showing the use of a computer	32
2.4 <i>Calibration Software</i>	32

1. Fundamentals

1.1 Characteristics of light

Light, the giver of life, has always held a great fascination for human beings. It is therefore no coincidence that people have been trying to find out what light actually is for a very long time. We can see it, feel its warmth on our skin, but we cannot touch it. The ancient Greek philosophers thought light was an extremely fine kind of dust, originating in a source and covering the bodies it reached. They were convinced that light was made up of particles. As humankind progressed and we began to understand waves and radiation, it was proved that light did not, in fact, consist of particles but that it is an electromagnetic radiation with the same characteristics as radio waves. The only difference is in the wavelength. We now know that the characteristics of light are revealed to the observer depending on how he sets up his experiment. If the experimenter sets up a demonstration apparatus for particles, he will be able to determine the characteristics of light particles. If the apparatus is one used to show the characteristics of wavelengths, he will see light as a wave. The question we would like to be answered is: What is light in actual fact? The duality of light could only be understood using modern quantum mechanics. Heisenberg showed, with his famous “uncertainty relation”, that strictly speaking, it is not possible to determine the place x and the impulse p of any given occurrence at the same time

$$\Delta x \cdot \Delta p_x \geq \frac{1}{2} \hbar$$

If, for example, the experimenter chooses a set up to examine particle characteristics, he will have chosen a very small uncertainty of the impulse p_x . The uncertainty x will therefore have to be very large and no information will be given on the course of the occurrence. Uncertainties are not given by the measuring apparatus, but are of a basic nature. This means that light always has the particular quality the experimenter wants to measure. We can find out about any characteristic of light as soon as we think of it. Fortunately the results are the same, whether we work with particles or wavelengths, thanks to Einstein and his famous formula:

$$E = m \cdot c^2 = \hbar \cdot \omega$$

This equation states that the product of the mass m of a particle with the square of its speed c corresponds to its energy E . It also corresponds to the product of Planck’s constant $h = \hbar \cdot 2\pi$ and its radian frequency $\omega = 2\pi \cdot \nu$. In this case ν represents the frequency of luminous radiation. In our further observations of the fundamentals of the Michelson interferometer, we will use the wave representation and describe light as electromagnetic radiation. All types of this radiation, whether in the form of radio waves, X-ray waves or light waves consist of a combination of an electrical field \vec{E} and a magnetic field \vec{H} . Both fields are bound together and are indivisible. Maxwell formulated this observation in one of his four equations, which describe electromagnetic fields

$$\nabla \times \vec{H} \approx \frac{\partial \vec{E}}{\partial t}$$

According to this equation, every temporal change in an electrical field is connected to a magnetic field (Fig.1).

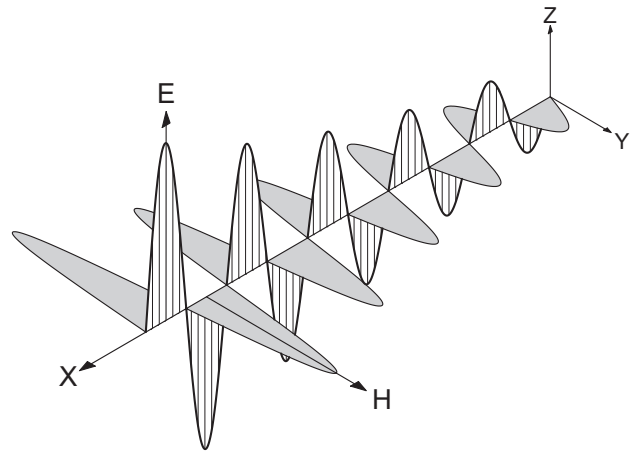


Fig. 1: Light as electromagnetic radiation

Due to the symmetry of this equation, a physical condition can be sufficiently described using either the electrical or the magnetic field. A description using the electrical field is preferred since the corresponding magnetic field can then be obtained by temporal derivation. In the experiments (as presented here) where light is used as electromagnetic radiation, it is advantageous to calculate only the electrical fields since the light intensity is:

$$I = \frac{c \cdot \epsilon}{4\pi} \cdot |\vec{E}|^2$$

This is also the measurable size as perceived by the eye or by a detector. In this case, the speed of light is c in the respective medium and ϵ is the corresponding dielectric constant. Since we are comparing intensities in the same medium, it is sufficient to use

$$I = |\vec{E}|^2$$

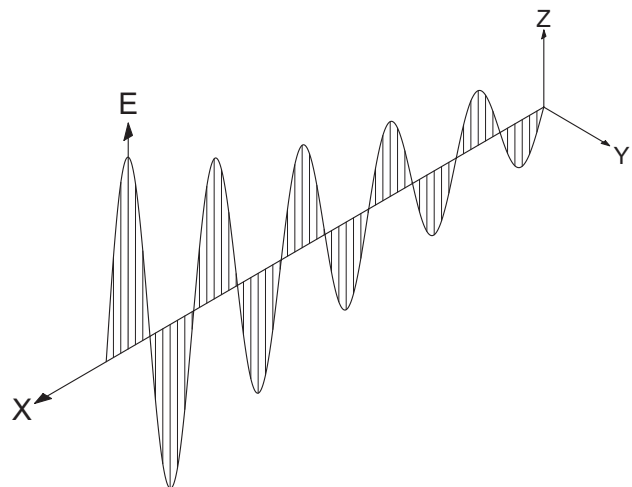


Fig. 2: In this experiment we need only observe the electrical field strength E

The experimental findings agree with the theory of electromagnetic radiation if a harmonic periodic function becomes temporally dependent on the field strength of light. In its simplest form this is a sine or cosine function. An

amplitude E_0 and a wavelength λ should be used in the definition of this kind of function. Let us begin with the equation:

$$E_x = E_0 \cdot \sin\left(\frac{2 \cdot \pi}{\lambda} \cdot x\right) \quad (1.1.1)$$

which we will elaborate and explain further.

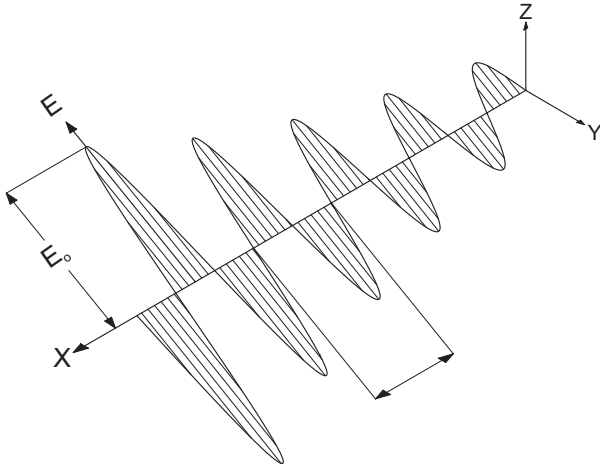


Fig. 3: Amplitude and wavelength

In the above figure the light wave no longer oscillates in the Z-direction as in Fig. 2 but at a certain angle to the Z- or Y-axis. The X-axis has been chosen as the direction of propagation of the wave. We still require information on the direction in which the electrical field strength E_x oscillates to complete the description of the wave. Strictly speaking, the field E_x oscillates vertically to the direction of propagation X. However, we have to give information regarding the Z- and Y-axis. This leads to the term 'Polarisation' and Direction of Polarisation. In Figs. 1 and 2 we used linearly polarised light with a polarisation direction in Z and in Fig. 3 we used a different direction. We will now introduce the polarisation vector P, which is defined in the following Fig. 4. We have to look into the light wave in the direction of the X-axis for this purpose.

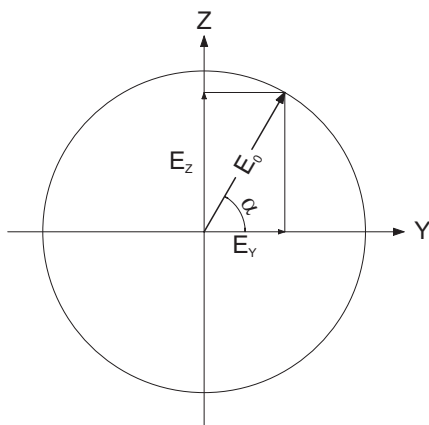


Fig. 4: Definition of the polarisation vector

We can observe a wave expanding in the X-direction and oscillating at the electrical field amplitude E_0 below an angle α to the Y-axis. The amplitude E_0 is separated into its components, which oscillate in the Z- or Y-direction. We now write \hat{E}_0 instead of E_0 to indicate that the amplitude E_0 is now made up of individual components.

$$\hat{E}_0^2 = (E_0^Y)^2 + (E_0^Z)^2 = (E_0^Y \cdot \hat{e}_Y + E_0^Z \cdot \hat{e}_Z)^2$$

In this case $\hat{e}_Z = (0,1)$, $\hat{e}_Y = (1,0)$ is the unit vector in the Z- or Y-direction on the ZY-plane. Characteristically the unit vectors yield $|\hat{e}_Z| = 1$ and the scalar product $\hat{e}_Z \cdot \hat{e}_Y = 0$. The equation (1.1.1) can now be generalised to:

$$E_x(Y, Z) = (E_0^Y \cdot \hat{e}_Y + E_0^Z \cdot \hat{e}_Z) \cdot \sin\left(\frac{2\pi}{\lambda} \cdot x\right)$$

At this point we come across a fundamental principle in classic wave theory, i.e. the principle of superimposition. A big word for the simple statement:

Every wave can be represented as the sum of individual waves.

In our example we had separated the wave as shown in Fig.4 into two individual waves, i.e. one that oscillates in the Z-direction and another in the Y-direction. We could just as well say that our wave was formed by the superimposition of these two individual waves. The word interference can also be used to mean superimposition. In this context our wave was formed by the interference of two individual waves. This is the basis for the functioning of the Michelson interferometer. An introduction to this interferometer now follows. For the time being, let us return to the polarisation vector.

The polarisation vector P is also a unit vector, which always points in the direction of the oscillation of the electrical field E_x

$$\hat{P} = \frac{\hat{E}_0}{|\hat{E}_0|} = \frac{E_0^Y}{E_0} \cdot \hat{e}_Y + \frac{E_0^Z}{E_0} \cdot \hat{e}_Z$$

or as is written for vectors

$$\hat{P} = \left(\frac{E_0^Y}{E_0}, \frac{E_0^Z}{E_0} \right)$$

The polarisation vector for a polarisation in the Z-direction (0°) would then be, for example:

$$\hat{P} = (0,1)$$

for a polarisation direction of 45° it would be:

$$\hat{P} = \frac{1}{\sqrt{2}}(1,1)$$

The equation of the wave with any given polarisation direction will thus be

$$\hat{E}_x(Y, Z) = \hat{P} \cdot E_0 \cdot \sin\left(\frac{2\pi}{\lambda} \cdot x\right), \text{ or}$$

$$\hat{E}_x(Y, Z) = (E_Y, E_Z) \cdot \sin(k \cdot x) \quad (1.1.2)$$

We have introduced the wave number k in the above equation

$$k = \frac{2\pi}{\lambda}$$

The wave number k has the length dimension⁻¹ and was originally introduced by spectroscopists because it was a

size that could be measured immediately with their equipment. We are using this size because it simplifies the written work.

Till now we have only described the wave as a function of the location. This would be sufficient in order to understand the classical Michelson interferometer, but not for technical interferometers. We carry out the following hypothetical experiment to introduce the "time coordinate":

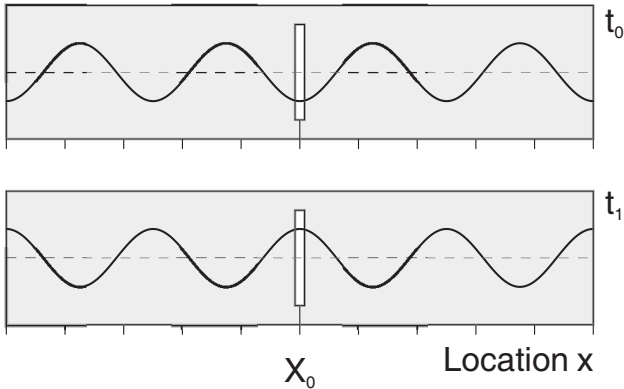


Fig. 5: Hypothetical experiment for the introduction of dependency on time

The talented physicist Walter S. * (*Names have been changed) is working on new experiments with electromagnetic waves in his laboratory. His colleague Gerd N. who is jealous of his rival's success sees that the door to Walter S.' laboratory has been left open a crack and uses the opportunity to find out what his colleague is working on. In spite of his nervousness, Gerd N. forces himself to make painstakingly accurate notes of his observations. He measures the time with his Swiss stop watch, a present from his father, who was also a physicist and notes the respective intensities of what he sees through the crack in the door. He rushes into his modest study, red in the face, and writes his observations into his laboratory records. Here we find the following entries:

".....I stood at location X and looked through the crack in the door. I observed periodic oscillations in field strength, which fluctuated between a maximum and a minimum. I began measuring at the time $t=0$, when the field strength was at its minimum. At the time t_1 I calculated the maximum field strength. The differences in time between the extreme values stayed constant." A graph of his measurement values follows:

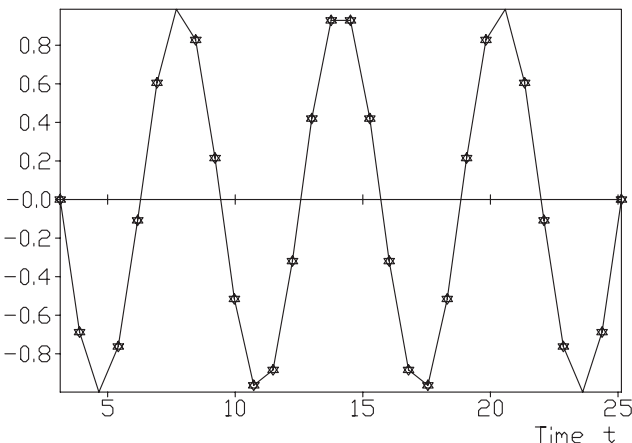


Fig. 6: Gerd N's measurement curve

Gerd N. further states that:"..... the time that passed between two maxima as the duration period t . I have observed n of such maxima within one second. Obviously

$$v = \frac{n}{\tau}$$

the field strength has a frequency of $\frac{n}{\tau}$ and follows a periodic function $E = E_0 \cdot \sin(2\pi \cdot v \cdot t)$ although this function begins with positive values. The measured values only correspond to the observations if a constant is added to the argument of the sine

$$E = E_0 \cdot \sin(2\pi \cdot v \cdot (t - t_0))$$

Some weeks later both colleagues meet at a specialists' conference. As is often the case, the evening session of the conference took place in a suitable atmosphere, where the participants committed themselves to the team spirit over a glass of wine and agreed on all other things as well. Walter S. spoke openly about how he had managed to formulate the position of the course of a wave and wrote his formula on the beer mat, commonly used in this area

$$E = E_0 \cdot \sin\left(\frac{2\pi}{\lambda} \cdot (x - x_0)\right)$$

How the evening finally ended is left to your own imagination. What is important is that both experimentalists measured the same field strength, one with a stopwatch in his hand, the other with a scale. Therefore

$$\frac{E}{E_0} = \sin(2\pi \cdot v \cdot (t - t_0)) = \sin\left(\frac{2\pi}{\lambda} \cdot (x - x_0)\right)$$

This is the same as

$$v \cdot (t - t_0) = \frac{1}{\lambda} \cdot (x - x_0)$$

or

$$v \cdot \lambda = \frac{(x - x_0)}{(t - t_0)} = c$$

This hypothetical experiment has shown us that we can describe the wave by its temporal course on the one hand, and by the position of the course of a wave on the other. We have also found out the importance of the relationship of the speed c of a wave to its frequency and wavelength

$$v = \frac{c}{\lambda}$$

If we write the relation with $\omega=2\pi v$ as a rotary frequency we get:

$$\omega = \frac{2\pi}{\lambda} \cdot c = k \cdot c$$

Let us now return to the generalised formula for the temporal and spatial course of the field strength of a light wave. Since the sine is a periodic function we can include the temporal and spatial dependency into the argument. We would then get

$$\hat{E}_x(Y, Z) = (E_Y, E_Z) \cdot \sin(k \cdot (x - x_0) + \omega \cdot (t - t_0))$$

If we now make the constants kx_0 and ωt_0 into one constant δ we obtain the general formula

$$\hat{E}_x(Y,Z) = (E_Y, E_Z) \cdot \sin(k \cdot x + \omega \cdot t + \delta) \quad (1.1.3)$$

1.2 Superimposition and Phase δ

δ is also described as a phase. Since this term is often inconvenient we would like to examine it more closely. If we put $x=0$ and $t=0$ into (1.1.3) the field strength will have a value of

$$\hat{E}_x(Y,Z) = (E_Y, E_Z) \cdot \sin(\delta)$$

and thus defines an initial value for the amplitude. This value is or will be determined according to the physical situation.

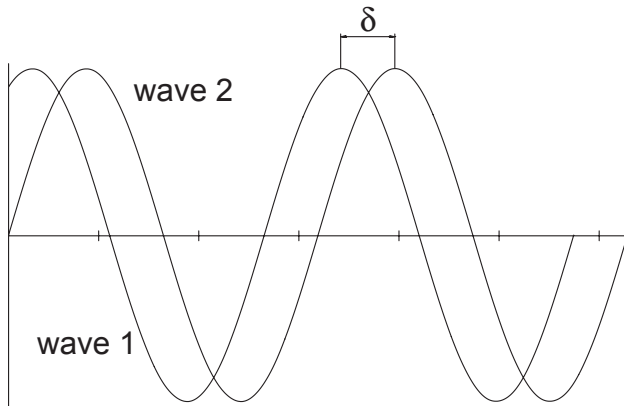


Fig. 7: Definition of phase δ

Obviously phase δ contains information about the relationship between two or more waves. Let us presume that the waves originate in a light source and phase δ contains information on how the wave was formed. Light waves are formed by emission processes. There is an emission procedure for every photon or light wave. Such processes are always taking place when the light source is continuously illuminated. The emission procedures are distributed statistically according to the type of light source. Thus, phase δ is also distributed statistically. If the emission procedures are coupled to each other, as is the case with lasers, and all photons or waves have the same frequency or wavelength (they are monochromatic) the light is then described as coherent (holding itself together). If, however, phase δ is randomly distributed, then this light is incoherent. This is the case with thermal light sources, e.g. light bulbs. To judge the coherence of a light source, the characteristics of the emitted waves and/or photons would have to be classified. The waves (photons) are first sorted out according to their frequencies (wavelengths) and then according to their phases. If we form small “containers” in our minds with the labels:

$$k = \frac{2\pi}{\lambda} = \text{numerical value and}$$

$$\delta = \text{numerical value}$$

and if we now sort out the photons in these containers and then count the photons per container, we could obtain a statement on the coherence. This kind of container is also called a phase cell. If all photons were in one container or phase cell, the light would be completely coherent. In the example according to Fig. 7 the wave 2 has a phase

of δ as opposed to the wave 1, in other words, the waves have a phase difference of δ , presuming that we have produced two such waves (this is exactly what the Michelson interferometer does). We expect a third wave through the principle of superimposition, which is formed by the superimposition or interference of the two basic waves. We will find out how this wave looks like by simply adding both basic waves:

$$\text{Wave 1} \quad \hat{E}_1(Y,Z) = (E_Y, E_Z) \cdot \sin(k \cdot x + \omega \cdot t + \delta)$$

$$\text{Wave 2} \quad \hat{E}_2(Y,Z) = (E_Y, E_Z) \cdot \sin(k \cdot x + \omega \cdot t)$$

$$\text{Wave 3} \quad \hat{E}_3(Y,Z) = \hat{E}_1(Y,Z) + \hat{E}_2(Y,Z)$$

It is now easy to imagine that a large number of waves with different frequencies ω or wavelengths λ and phases δ result in such a mixture and that it makes little sense to carry out superimposition or interference experiments with this light. Therefore light sources which emit light within a narrow emission spectrum with a phase as constant as possible are selected. Lasers are an example of such light sources. But when Michelson carried out his experiments around 1870 he could not use lasers. He used the red emission line of a cadmium lamp whose emission bandwidth showed a coherence length of only 20 cm. This means that when, for example, waves at the position $x=0$ were superimposed with those at the position $x=20$, there was no readable interference any more. We will come back to the important term “*coherence length*” later on and discuss it in more detail.

1.3 Interferometer

An apparatus that produces this physical condition is shown in the following diagram.

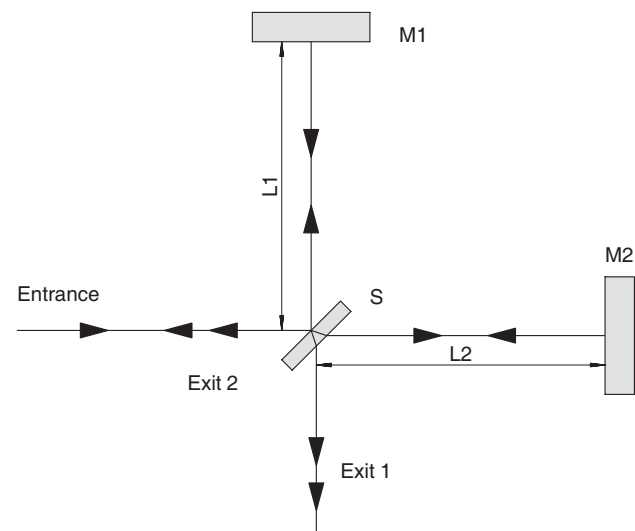


Fig. 8: Michelson interferometer.

We beam light into the entrance of the interferometer from some light source. The light is split into two bundles on a beam-splitting plate S . One bundle hits the mirror $M1$ and the other the mirror $M2$. The bundles will reflect back in themselves at these mirrors and reunite at the beam-splitting plate S . The respective bundles are split into two further bundles due to the characteristics of the beam-

splitting plate and one bundle is led in the direction of exit 1, the other in the direction of exit 2 in the process. Exit 2 of the Michelson interferometer points in the direction of the light source, so this exit is practically of no use to us to set up photodetectors or imaging screens. This is why only exit 1 will be mentioned. However, exit 2 must also be taken into consideration for the energy balance. Whatever technical model of an interferometer is chosen, it can be represented easily in an optically circuit diagram.

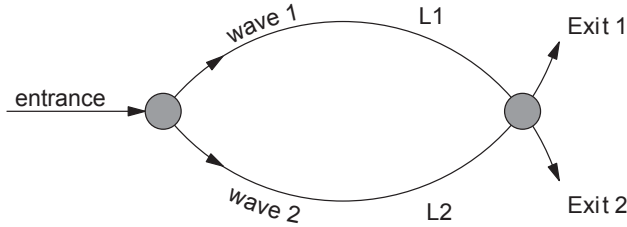


Fig. 9: "Optical circuit diagram" of an interferometer

The light, which is put into the entrance of the interferometer, is split into two bundles. How this happens technically is not important for the time being. This kind of element can generally be called a directional coupler. Bundle 1, or, in the simplest case the wave 1 runs through the path L1 and the other wave 2 runs through the path L2. Both waves are brought together in a mixer. This mixer has two exits. In the Michelson interferometer directional couplers and mixers are one and the same element. We are only interested in exit 1 for the time being. As we will see later on, exit 2 is symmetrical to exit 1. We now just have to calculate wave 3 at exit 1 which is formed out of the superimposition of wave 1 with wave 2 which have travelled along a path from L1 or L2. Without jeopardizing the general validity of the solution, we can assume that the electric field strength only oscillates in the Y-direction. As already defined in the beginning the waves propagate in the X-direction. Although the direction of the bundle of rays can point in other directions after separation, they should have the same direction of propagation, at least in the mixer, if they are to interfere at all.

$$\text{Wave 1} \quad E_1 = E_{01} \cdot \sin(k \cdot L_1 + \omega \cdot t)$$

$$\text{Wave 2} \quad E_2 = E_{02} \cdot \sin(k \cdot L_2 + \omega \cdot t)$$

$$\text{Wave 3} \quad E_3 = E_1 + E_2$$

Since both waves E_1 and E_2 are formed when the entering wave E_0 is split and the splitter should separate them symmetrically, both partial waves do not have any phase shift δ with regard to each other.

$$E_3 = E_{01} \cdot \sin(k \cdot L_1 + \omega \cdot t) + E_{02} \cdot \sin(k \cdot L_2 + \omega \cdot t)$$

A screen or photodetector is installed at exit 1. The human eye and the photodetector are not in a position to register electric field intensities, but can only register the light intensity I which is connected to the field strength:

$$I = E^2$$

$$I = \left(E_{01} \cdot \sin(k \cdot L_1 + \omega \cdot t) + E_{02} \cdot \sin(k \cdot L_2 + \omega \cdot t) \right)^2$$

$$I = E_{01}^2 \cdot \sin^2(kL_1 + \omega t) + 2E_{01}E_{02} \sin(kL_1 + \omega t) \sin(kL_2 + \omega t) + E_{02}^2 \cdot \sin^2(kL_2 + \omega t)$$

To simplify the mixed term we use the relation:

$$2 \cdot \sin \alpha \cdot \sin \beta = \cos(\alpha - \beta) + \cos(\alpha + \beta)$$

and obtain:

$$I = E_{01}^2 \cdot \sin^2(kL_1 + \omega t) + E_{01}E_{02} \cos(k(L_1 - L_2)) + E_{01}E_{02} \cos(k(L_1 + L_2) + 2\omega t) + E_{02}^2 \cdot \sin^2(kL_2 + \omega t)$$

The expression for light intensity, which is perceived either by a detector or by our own eyes, consists of four terms. Only the second term is not dependent on the time t . All other terms oscillate with the frequency ω . We use

$$\omega = 2\pi\nu = 2\pi \frac{c}{\lambda}$$

to determine this ω . The frequency of light is ν and has a wavelength λ and a speed c . In the later experiments we will select the light emitted by a Helium-Neon laser. The wavelength of this light is 633 nm. Using this value and the speed of light $c = 3 \times 10^8$ m/s the frequency ν is calculated as:

$$\nu = \frac{3 \cdot 10^8}{633 \cdot 10^{-9}} = 4,7 \cdot 10^{14} \text{ Hz}$$

The sine of the first and last term oscillates at this frequency and the third even oscillates at double this frequency. Neither the eye nor any photodetector is capable of following this extremely high frequency. The fastest photodetectors nowadays can follow frequencies of up to approx. 2×10^9 Hz. This is why a detector, and even more so, our eyes can only perceive average values. The \sin^2 terms oscillate between 0 and 1; its temporal average value is therefore 1/2. The cosine term oscillates between -1 and +1, the average value is zero. The intensity I would therefore be:

$$I = \frac{1}{2} E_{01}^2 + \frac{1}{2} E_{02}^2 + E_{01}E_{02} \cos(k \cdot \Delta L)$$

$$\Delta L = L_1 - L_2$$

Obviously I is maximum if the cosine is one. This is always the case when its argument is zero or an integral multiple of 2π . I is minimum just at the time when the cosine is -1

$$I_{\max} = \frac{1}{2} E_{01}^2 + \frac{1}{2} E_{02}^2 + E_{01}E_{02} = \frac{1}{2} (E_{01} + E_{02})^2$$

$$I_{\min} = \frac{1}{2}E_{01}^2 + \frac{1}{2}E_{02}^2 - E_{01}E_{02} = \frac{1}{2}(E_{01} - E_{02})^2$$

Let us remind ourselves that

$$k = \frac{2\pi}{\lambda}$$

and that it is constant at a stable wavelength. The light intensity at exit 1 is therefore obviously only dependent on the path difference L_1-L_2 . If both paths having the same length, both partial waves interfere constructively and the light intensity observed is maximum. If the path difference is just $\lambda/2$ then:

$$k \cdot \Delta L = \frac{2\pi}{\lambda} \cdot \frac{\lambda}{2} = \pi$$

The cosine is then -1 and the light intensity I at the exit becomes minimum. Let us divide the initial intensity into two partial ones of equal size, i.e. E_{01} and E_{02} . In this case even the light intensity is zero. Here, both partial waves interfere destructively. Keeping in mind that the wavelength for our experiment is 633 nm and that it leads to a shift from one wave to another by only $\lambda/2=316.5$ nm = 0.000000316 mm (!) from a light to a dark transition at exit 1, this type of interferometer is a highly precise apparatus for measuring length.

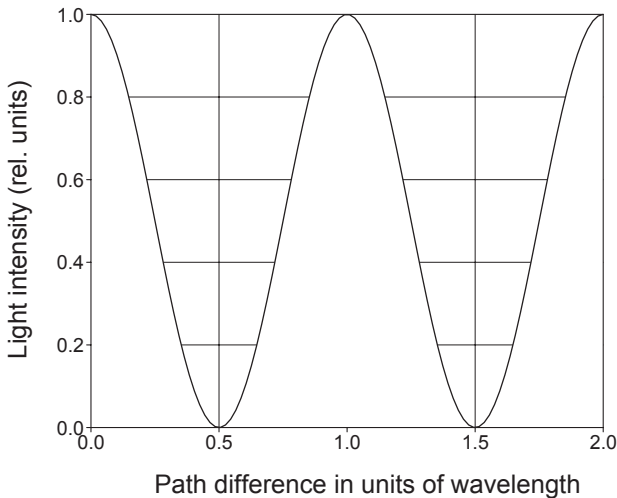


Fig. 10: Interferogram, light intensity versus path difference

1.4 Real interferometer

In the preceding chapter, we assumed that we had ideal light sources and optical components at our disposal. Practical interferometry is, in fact, characterised by these components. Michelson (1871) did not construct his interferometer to examine the interference of light, but to prove the ‘world ether’ theory. It was therefore an optical instrument that underwent constant development. Since the interference fringes had to be judged with the naked eye, it was the aim of this further development to maximise the contrast in light and dark shades.

1.4.1 Contrast or visibility

Michelson defined as a scale for the measurement of contrast:

$$V = \frac{I_{\max} - I_{\min}}{I_{\max} + I_{\min}}$$

Historically, the word visibility or clarity was also chosen for contrast.

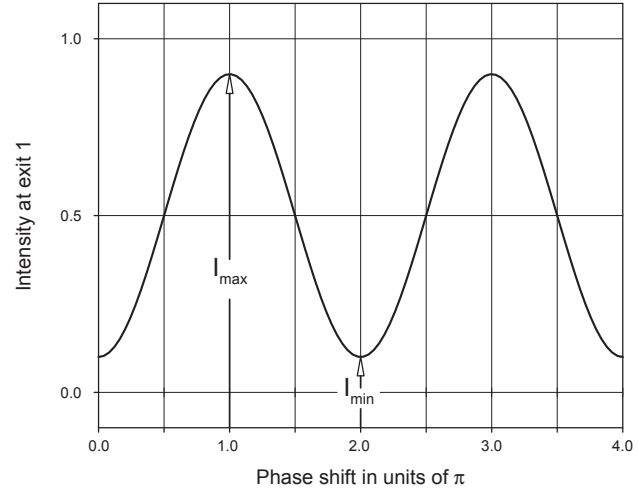


Fig. 11: Signal at exit 1 at $I_{01} = 0.2 I_0$ and $I_{02} = 0.8 I_0$

If, for example, the splitting relationship of the beam splitter is not exactly 1 then the interferogram will change as shown in Fig.11.

Using

$$I_{\max} = \frac{1}{2}I_{01} + \frac{1}{2}I_{02} + \sqrt{I_{01} \cdot I_{02}}$$

and

$$I_{\min} = \frac{1}{2}I_{01} + \frac{1}{2}I_{02} - \sqrt{I_{01} \cdot I_{02}}$$

we obtain

$$V = \frac{2 \cdot \sqrt{I_{01} \cdot I_{02}}}{I_{01} + I_{02}} = \frac{2 \cdot \sqrt{I_{01} \cdot I_{02}}}{I_0}$$

for the contrast. According to Fig.10 the contrast is $V=1$ and in Fig.11 $V=0.8$. A contrast reduction also occurs if, for example the adjustment is not optimal, i.e. the overlap of both the interfering rays is not 100 %. In this case

$$I_{01} + I_{02} < I_0$$

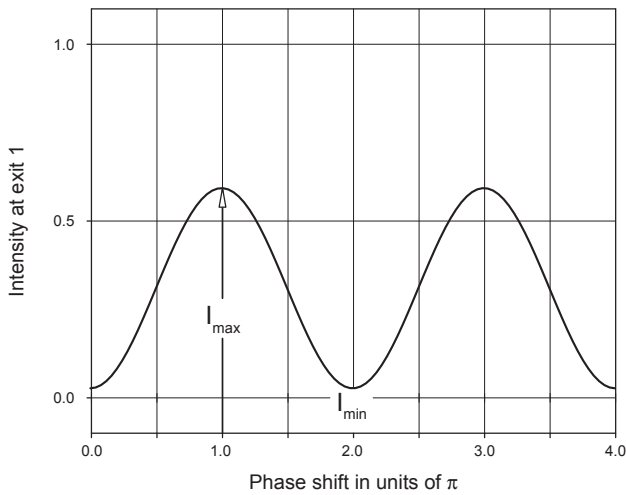


Fig. 12: Interference signal at exit 1 at $I_{01} = 0.2 I_0$ and $I_{02} = 0.4 I_0$, caused by maladjustment and a beam splitter which is not ideal.

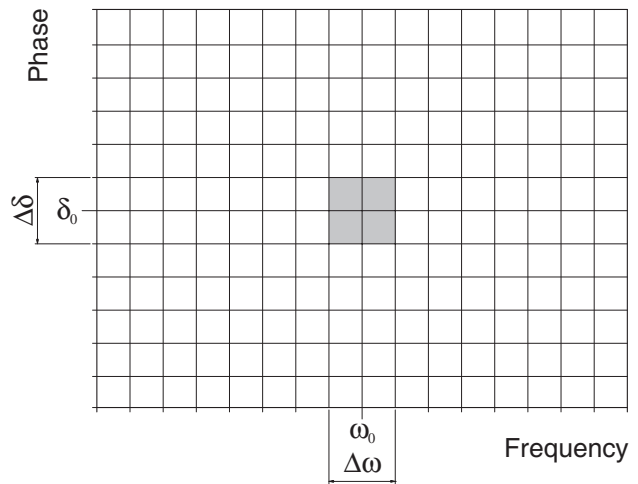


Fig. 13: Light, whose photons originate from the smallest possible phase cell according to Heisenberg’s uncertainty principle, is coherent.

1.4.2 Light sources and coherence

Till now we have tacitly assumed that the light source only has a sharp frequency ω . This is never the case in practice. We would therefore like to examine the influence of the spectral emission of the light source on interference formation. Radiation that gets its energy from the warmth of a radiating body is known as thermal radiation and is sent out by glowing solids (metal, coal etc.) or gases at high pressures. But radiation can also be produced without extracting energy from the warmth of a medium, e.g. by introducing electrical energy (discharge in gas). In this type of radiation production, the temperature of the radiator (except in loss mechanisms) does not change. The light produced in this way is known as “cold light” or also luminous radiation. The type of emission depends on the excited electronic or vibronic states of the atoms and molecules concerned. Light sources that emit light based on these mechanisms are an important component of modern light technology. Whereas light bulbs are thermal radiators, fluorescent lamps, gas discharge lamps, monitors as well as lasers are sources of cold light.

Classic optics states that light is coherent when it shows signs of interference. The narrower the emission line width $D\omega$ is the higher will be the contrast observed in this process. There is obviously a connection between the contrast or visibility V of the interferogram and the line width of the light source used.

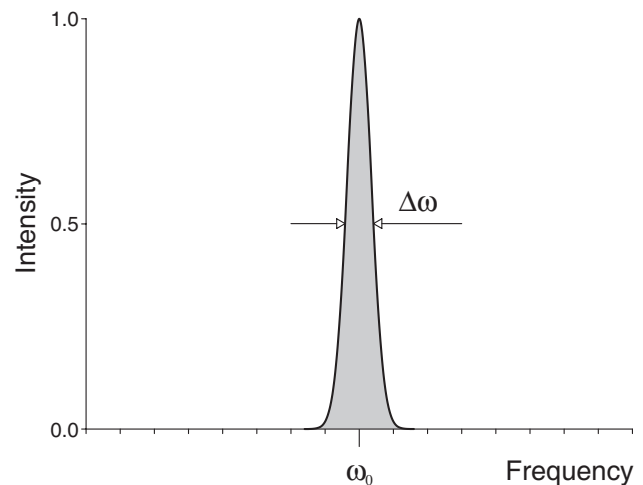


Fig. 14: Light with a narrow band emission with emission bandwidth $D\omega$.

1.5 Coherence

In classic optics, light was described as coherent if it could produce interferences. The term coherence was elaborated by the photon statistics introduced by quantum optics. It says, that light is coherent when photons originate in the same phase cell, that is; they have the same frequency and phase within Heisenberg’s uncertainty principle. Monochromatic light is only coherent if the partial waves also have the same phases.

If we follow the views of classic optics in the next chapters, this is because we will not touch the limits of Heisenberg’s uncertainty principle by far, in spite of using a laser as the light source for the interferometer. The emission bandwidth and the emitted line width of the technical HeNe laser used is very big compared to the theoretical natural bandwidth of a line.

1.6 Thermal light

We know from our daily observations that a hot body transmits light radiation. The higher the temperature of the body, the whiter the light seems.

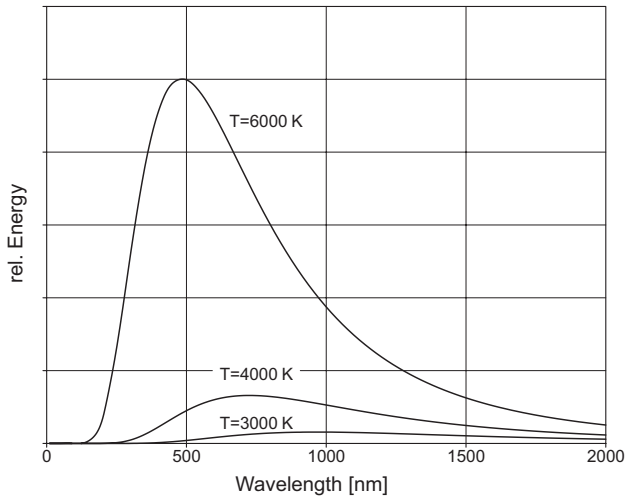


Fig. 15: The spectral distribution of a black body radiator (thermal radiator, Planck’s radiation law) for various temperatures

It can thus be concluded that this kind of radiator has a very large emission bandwidth $\Delta\omega$. Therefore thermal light sources are not suitable for interferometry.

1.7 Cold light

Another type of light production is the light emission of atoms and molecules, which show a clear spectral structure characteristic of certain atoms, and molecules, contrary to the continuous radiation of the temperature radiators. Apart from their characteristics as a light source, the main interest in spectra was to use them to find out more about the structure of atoms and molecules.

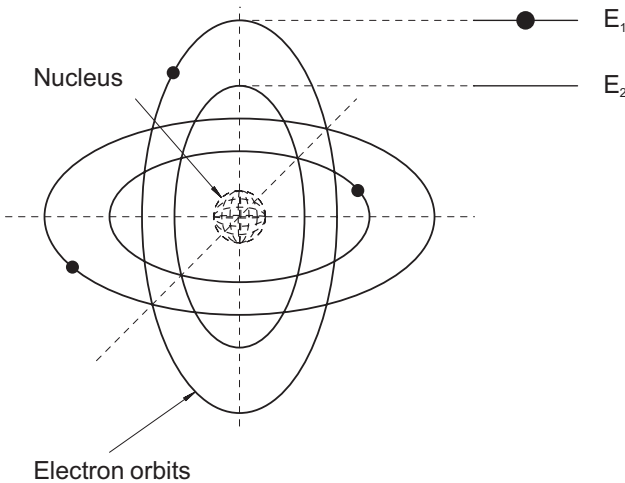


Fig. 16: Bohr’s idea of the atom

Einstein elaborated Bohr’s theories on the atom model to the extent that light emitted or absorbed from the atoms can only have energies of $E_2 - E_1 = h\nu$ (Fig.16). His work and measurements proved that both in a resonant cavity and in the case of atomic emission discrete energies must be assumed. Einstein started off by trying to find one single description for these two types of light sources. He found the solution to this problem in 1917 when he derived Planck’s hypothesis once more in his own way. Photons or a radiation

field are produced through the transition from $2 \rightarrow 1$. With regard to what we have already considered, the frequency of the radiation produced in this way should actually be determined by $E_2 - E_1 = h\nu_0$. However, keeping in tune with Heisenberg’s uncertainty principle

$$\Delta x \cdot \Delta p_x \geq \frac{1}{2} \hbar \quad \text{or} \quad \Delta E \cdot \Delta t \geq \frac{1}{2} \hbar$$

which states that every emission process is affected by an uncertainty and the emission line therefore always has a certain width $\Delta\omega$.

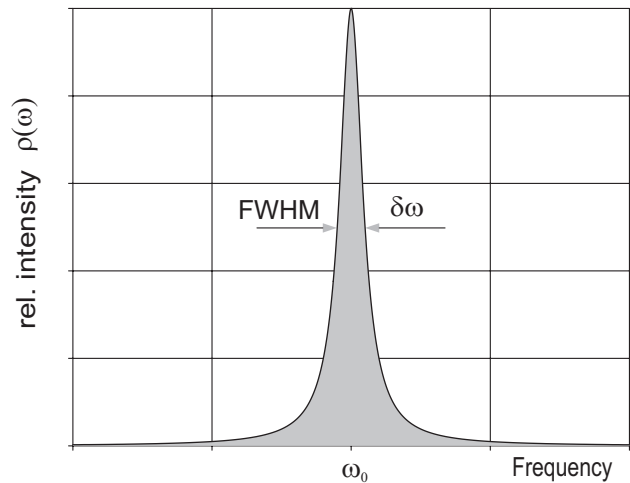


Fig. 17: Natural line width

$$\rho(\omega) = \frac{1}{(\omega - \omega_0)^2 + (1/2 \cdot \tau_s)^2}$$

This type of curve represents a Lorentz curve. Here, ω_0 is the resonant frequency and

$$\tau_s = \frac{1}{A_{21}}$$

is the average life of state 2. The half-width value $\delta\omega$ (or also FWHM, Full Width at Half Maximum) of the curve according to Fig. 17 is calculated by inserting the value for $\rho(\omega) = 1/2$. We find that

$$\delta(\omega)_{\text{nat}} = A_{21} \tag{1.7.1}$$

is the natural line width of a transition, defined by the Einstein coefficient A_{21} , which has a particular value for every transition. The results gained can also be interpreted to mean that state 2 does not have any sharply defined energy but an expansion with a half-width value of $\Delta E = 2\pi h A_{21}$. There would therefore be some uncertainty in this state. Quantum mechanics has shown that this effect is of fundamental importance. It has been called the Heisenberg’s uncertainty relation after its inventor. In normal optical transitions, the value of τ_s is between 10^{-8} and 10^{-9} sec. This lifetime, determined by the spontaneous transitions alone is a decisive factor for the so-called natural half-width value of a spectral line. Regarding descriptions, it must be stressed at this point that we must differentiate between the width of a state and the width of a line as well as between the terms state and line. Atomic states always exist, so no statement will be made on whether the state is occupied or empty. A line can only be formed if, for example,

an emission occurs by the transition from the state from to 2→1. The line is a word used by spectroscopists. They may produce, for example, photographic plates using their spectral apparatus, on which fluorescent light is shown divided up into its wavelengths. They use slits in the optical radiation path for an easy evaluation of the spectra. Fig 18 shows this kind of line spectrum.



Fig. 18: Photograph of the emission of a light source with the corresponding energy level showing a so-called line spectrum.

The spectrum according to Fig.18 can be seen from the line widths as well as from the emission wavelengths. Please note, however, that the measurement apparatus makes the line widths appear larger than they actually are.

If the spectral distribution of a line radiator were carried into that of the thermal radiator, the result would be a narrower line than the one in Fig.15.

Let us return to the influence of the spectral bandwidth $\Delta\omega$ on the contrast of our interferometer. To make it easier we have selected the intensities as

$$I_{01} = I_{02} = \frac{1}{2} \cdot I_0$$

and obtain for the intensity of the interfering waves:

$$I = I_0 \{1 + \cos(k \cdot \Delta L)\}$$

However, now the intensity I_0 is a function of ω :

$$I_0 \rightarrow \hat{I}(\omega) = \hat{I} \cdot \rho(\omega) \cdot \partial\omega$$

So, we must integrate over all ω :

$$I = \int_{-\infty}^{+\infty} \{ \hat{I} \cdot \rho(\omega) + \hat{I} \cdot \rho(\omega) \cdot \cos(\omega / c \cdot \Delta L) \} \cdot \partial\omega$$

and obtain for the interferogram

$$I = I_0 + \int_{-\infty}^{+\infty} \hat{I} \cdot \rho(\omega) \cdot \cos(\omega / c \cdot \Delta L) \cdot \partial\omega \quad (1.7.2)$$

We can obtain the contrast or the visibility of the interference from the extreme values of (1.7.2):

$$V(\Delta L) = \frac{I_{\max} - I_{\min}}{I_{\max} + I_{\min}}$$

Thus the contrast function V , which is still dependent on ΔL after the integration, is the envelope of the interferogram $I(\Delta L)$. According to the form the emission line takes, or how the function $\rho(\omega)$ is made up, we can obtain the contrast of the function of the path difference ΔL and the corresponding contrast function $V(\Delta L)$ by using the above integration. The emission line of the laser, which we will use in the later experiment, can be described using a Gaussian function with a bandwidth $\Delta\omega$. The integral according to (1.7.2) can be calculated in this way. Counting over is carried out in [1] and the contrast function is shown

in the following diagram.

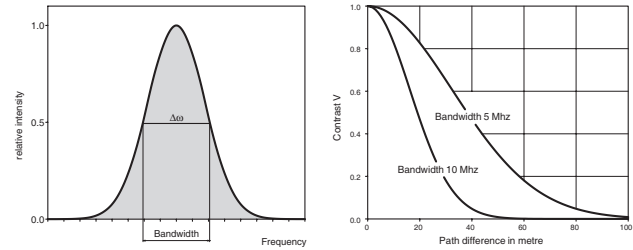


Fig. 19: Contrast as a function of the path difference of a light source with an emission bandwidth of 5 or 10 MHz (Laser).

The diagram on the right hand side of Fig.19 shows the contrast function. It shows that the contrast in a Gaussian distribution curve gradually drops as the path difference between both interfering waves increases. Theoretically, if the path difference is infinitely long, the contrast will eventually be zero. However this is not a practical answer. Although technical interferometers are being used for a long time there is no information on a marginal contrast, which merits an evaluation. We have therefore taken the liberty of defining the marginal contrast ourselves. We would say that if the contrast V has dropped to

$$\frac{1}{e^2} \cdot V_{\max} \approx 0,14$$

the practical coherence length L_e has been reached. Since these associations are important, we should now examine the practical conditions in more detail in anticipation of the experiments that are still to come. In the course of our studies, we had taken a partial ray from a ray of light at a location situated at any given distance from a light source. We will give the coordinate Z_1 to this location. Another partial ray is taken from a second location with the coordinate Z_2 . Both the partial rays are joined together and the intensity of the superimposed ray is measured.

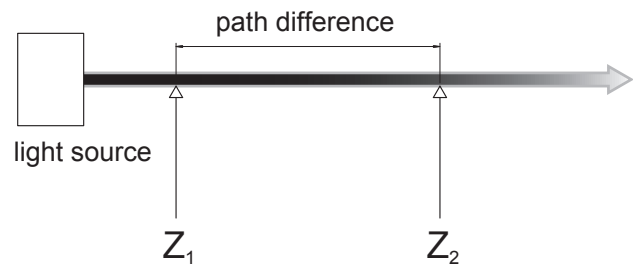


Fig. 20: Definition of coherence time

The photons taken from location z_2 have to travel a longer path than the photons at location z_1 . Since all photons fly at the speed of light c , the photons at location z_2 must have been “born” earlier than those at z_1 . The time difference between both photon generations is obviously

$$\Delta t = \frac{\Delta L}{c}$$

If we choose a path difference ΔL , that is large enough to cause a drop in contrast to the value we defined, then the corresponding running time Δt will be known as the coherence time. We have introduced this term for didactic reasons. It is not required in our further observations. The

construction according to Fig. 20 has a considerable disadvantage in that it cannot be carried out practically. The simplest basic form of a regulatory device for interference is the Michelson interferometer. Although the physical situation we have just discussed is the same, the path difference must be observed more closely.

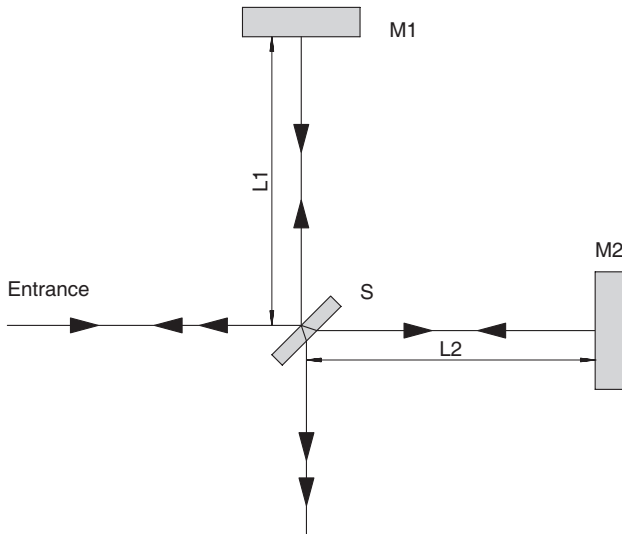


Fig. 21: Calculating the path difference ΔL using the Michelson interferometer

The beam splitter S splits the incoming beam. This is the origin of our system of coordinates. The mirror $M1$ should always be static, whereas the mirror $M2$ should be movable. Thus the two radiation paths form two arms of the interferometer. The one with the static mirror is known as the reference arm and the one with the movable mirror is the index arm. The partial beam in the reference arm travels a path of $2 L_1$ before it returns to the reunification point at the beam splitter S . The path $2L_2$ is crossed in the reference arm. The path difference is therefore:

$$\Delta L = 2 \cdot (L_2 - L_1)$$

We assume that the thickness of the beam splitter plate is zero. If $L_2 = L_1$, the path difference is zero. This can be adjusted for any number of intervals between the mirrors. In this state, the Michelson interferometer is symmetrical and even white light produces an interference pattern. This type of interferometer is sometimes also known as a white light interferometer. To find out the coherence length of the light source, the path difference is increased by shifting the mirror $M2$. There should be no maladjustment while doing this, since this will also reduce the contrast. If we measure this contrast as a function of the path difference, we get the contrast function. The point, at which the contrast is below the value already given by us, is the point where the coherence length has been reached. The following interference patterns would probably be seen on a screen.

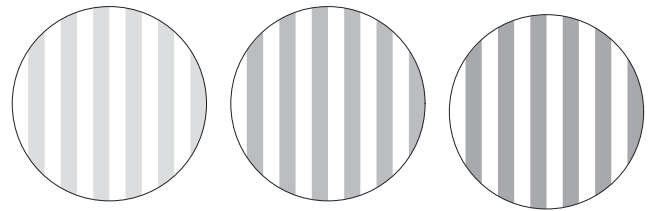


Fig. 22: Decreasing contrast with an increase in path difference.

Michelson carried out his experiments with the red line of a cadmium lamp that had a coherence length of only 20 cm. Since the index arm is crossed twice he had a measurement area of only 10 cm at his disposal. By measuring the contrast function, it is possible to find out the line width of the light source with (1.7.2). Can you imagine that Michelson carried this out with the green Hg line and saw 540,000 wavelengths in path difference with his naked eye, Perot and Fabry saw 790,000 and Lummer and Gehrcke as much as 2,600,000! Try and picture this process: The shifting of the measurement reflector, observing the light and dark band with the naked eye and counting to 2,600,000 at the same time. Till now we have examined the situation where the light source has different emission bandwidths but only one individual emission line. If we use a laser as a light source, the emission can consist of several so called ‘longitudinal oscillation modes’, as long as we do not take specific measures to produce only one. In the following experiment a laser is used which emits only two modes. Each of the two modes has a narrow bandwidth (approx. 2 MHz) but both modes have a difference in frequency of 900 MHz.

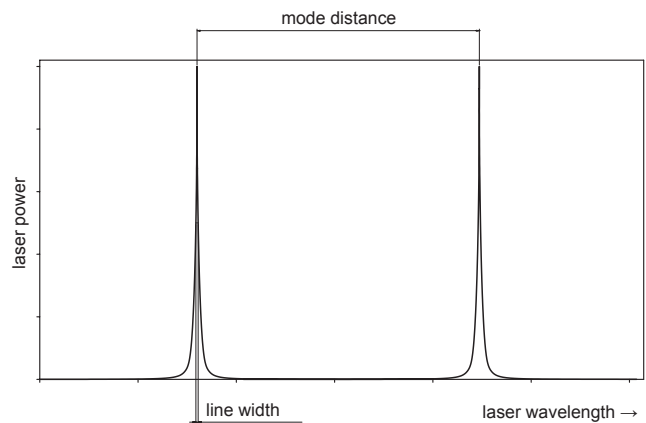


Fig. 23: Emission spectrum of the two-mode HeNe laser used

The expected interferogram will consist of a superimposition of the waves with both the frequencies ω and $\delta\omega$.

$$I = I_0 \cdot \left\{ 1 + \frac{1}{2} \cos\left(\frac{\omega}{c} \cdot \Delta L\right) + \frac{1}{2} \cos\left(\frac{\omega + \delta\omega}{c} \cdot \Delta L\right) \right\}$$

We can form a picture of the contrast function without having to make an explicit evaluation of the integral according to (1.7.2) by discussing the interferogram for some values of ΔL , using

$$\cos \alpha + \cos \beta = 2 \cdot \cos\left(\frac{\alpha + \beta}{2}\right) * \cos\left(\frac{\alpha - \beta}{2}\right)$$

$$I = I_0 \left\{ 1 + \cos\left(\frac{2\omega + \delta\omega}{2c} \cdot \Delta L\right) \cdot \cos\left(\frac{\delta\omega}{2c} \cdot \Delta L\right) \right\}$$

Since $\omega \gg \delta\omega$

$$I = I_0 \left\{ 1 + \cos\left(\frac{\omega}{c} \cdot \Delta L\right) \cdot \cos\left(\frac{\delta\omega}{2c} \cdot \Delta L\right) \right\}$$

Since $\delta\omega$ is not dependent on ω , this term is constant as far as the integration of all wavelengths is concerned and the contrast function of the single mode emission $V_1(\Delta L)$ becomes:

$$V_2(\Delta L) = V_1(\Delta L) \cdot \cos\left(\frac{\delta\omega}{2c} \cdot \Delta L\right)$$

The contrast function resulting from the two-mode emission is reproduced by the single mode emission, but the periodicity $\delta\omega/2$ superimposes with the cosine. The contrast is therefore zero for

$$\frac{\delta\omega}{2 \cdot c} \cdot \Delta L = (2n + 1) \cdot \frac{\pi}{2}, n = 0, 1, 2, \dots$$

or

$$\Delta L = (2n + 1) \cdot \frac{c}{\delta\omega}$$

The intervals between the zero points is exactly

$$\Delta L = \frac{c}{2 \cdot \delta\nu}$$

Let us remind ourselves of the interval in frequencies of longitudinal modes of a laser resonator:

$$\delta\nu = \frac{c}{2 \cdot L}$$

In this case L is the interval between the laser mirrors, so the interval between the zero points of the contrast corresponds exactly to the resonator length of the two-mode laser used.

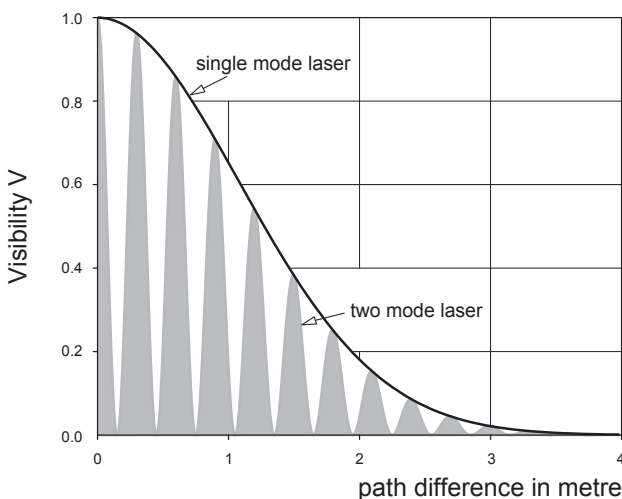


Fig. 24: Contrast as a function of the path difference of a single mode and a two-mode laser

Although the radiation is coherent, there is a disappearing contrast. In this case, it is not due to a lack of coherence, but to the phenomenon of optical interference. If the laser emission is put onto a photodetector at a suitably fast speed, we will have direct proof of optical interference. Optical

interference can be demonstrated using an oscilloscope or a spectrum analyser. However, this would mean that when a two-mode laser is used in interferometry the available measurement area of the index arm would be limited to $L/2$. Although the contrast does increase when this value is exceeded there is no information available during the zero crossings.

1.8 Wave fronts

The planes at which light has the same phases in a spatially wide radiation emission are known as wave fronts.

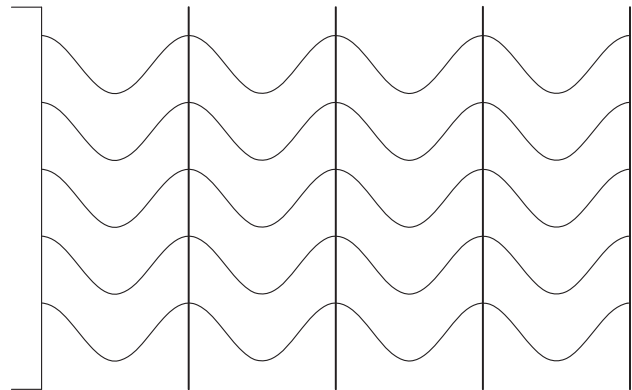


Fig. 25: Plain wave fronts of a parallel light bundle

If the light spreads itself in a parallel fashion, the planes of identical phases will be plane and therefore the wave fronts are called plane.

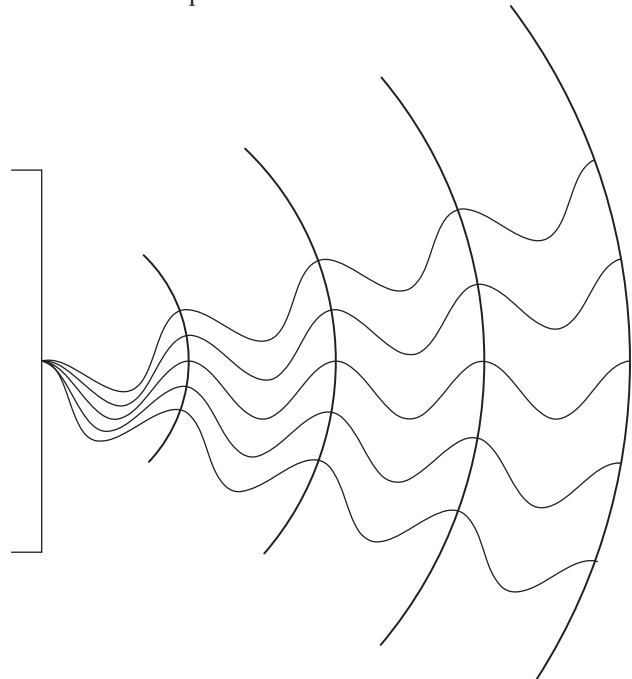


Fig. 26: Curved wave fronts of a divergent light bundle

However, if the radiation expansion is divergent, the wave fronts will be curved. If the radiation spreads in a solid angle with the same divergence in all directions, the wave fronts look like the surface of calotte shells. If two parallel light bundles are superimposed with plane wave fronts, we will see only brightness or darkness on a screen according to the relationship of the phases of the waves. If both bundles are attracted to each other there will be a striped pattern.

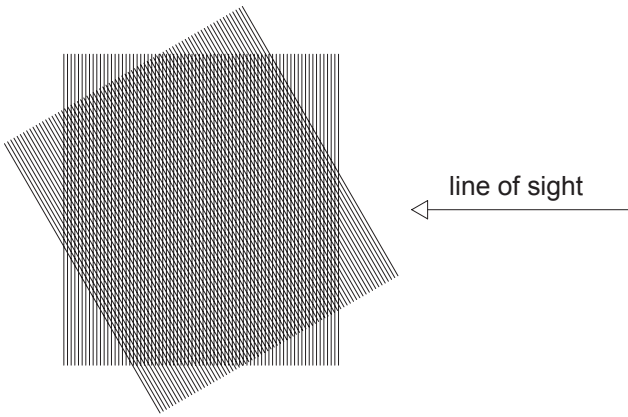


Fig. 27: Two light bundles attracted to each other with plane wave fronts

If one plane of a wave front, which represents the maximum of the field strength, cuts the plane of the minimum of a second wave front, then these are the locations for destructive interference. Since the wave fronts in the example according to Fig. 26 represent planes these intersecting points are on a straight line.

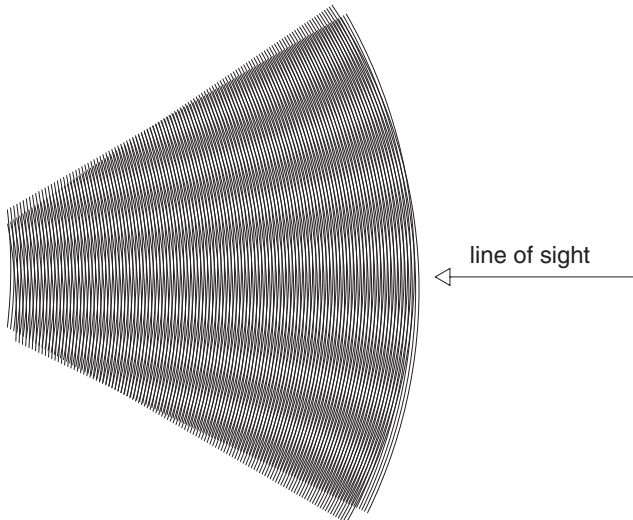


Fig. 28: Superimposition of two divergent light bundles

If, however, two light bundles with a slight divergence are superimposed, the intersecting points of the field strength minima or maxima lie on circles in space. A ring structure is formed.

1.9 Gaussian beams

In reality, there are no actual parallel light bundles and even wave fronts also only exist at a particular point. The cause for the failure of geometric optics lies in the fact that they were established at a time when people did not yet know that light is an electromagnetic wave and that its behaviour could therefore be described using Maxwell's equations. We will again use the wave equation already known to us for this purpose

$$\Delta \vec{E} - \frac{n^2}{c^2} \cdot \frac{\partial^2 \vec{E}}{\partial t^2} = 0$$

If light were limitless, it would spread itself in all directions in space as a spherical wave.

$$\vec{E} = \vec{E}(\mathbf{r}) \text{ with } r^2 = x^2 + y^2 + z^2$$

If, however we are interested in the technically important

case of the spherical wave spreading in direction z in a small solid angle then the solution is an equation for the electrical field

$$\vec{E} = \vec{E}(\mathbf{r}, z) \text{ with } r^2 = x^2 + y^2 + z^2$$

The solution to the wave equation is found in fields, which show a Gaussian shaped intensity distribution over the radiation cross-section and are therefore called Gaussian beams. According to the existing marginal conditions, Gaussian beams can be found in various modes. Such beams, especially the Gaussian basic mode (TEM_{00}) are preferably produced by lasers. However, the light coming from any light source can be seen as a superimposition of many such Gaussian modes. But the intensity of a pure mode is very small compared to the total intensity of a light source. The situation is different with lasers where the whole light intensity can be produced in the basic mode alone. This, as well as the monochromatic nature of laser radiation, is the main difference compared to conventional light sources. A Gaussian beam always has a beam waist. The beam radius w (w =waist) is a result of the solution of the wave equation

$$w(z) = w_0 \cdot \sqrt{1 + \left(\frac{z}{z_R}\right)^2}$$

w_0 is the smallest beam radius of the beam waist and z_r is the Rayleigh length.

Fig. 29 shows the course of the beam diameter with respect to the length z .

$$z_R = w_0^2 \frac{\pi}{\lambda}$$

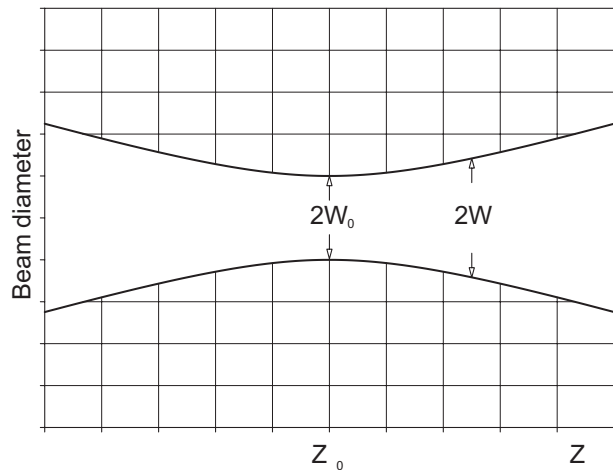


Fig. 29: Beam diameter of a Gaussian beam in the basic mode TEM_{00} as a function of the location z .

The beam spreads itself in the z -direction. At the point when $z=z_0$ the beam's radius is at its smallest. As the interval increases, the beam radius grows linearly. Since Gaussian beams are spherical waves, there is a radius of curvature R can be calculated using the following equation:

$$R(z) = z + \frac{z_r^2}{z}$$

This situation is shown in Fig.29.

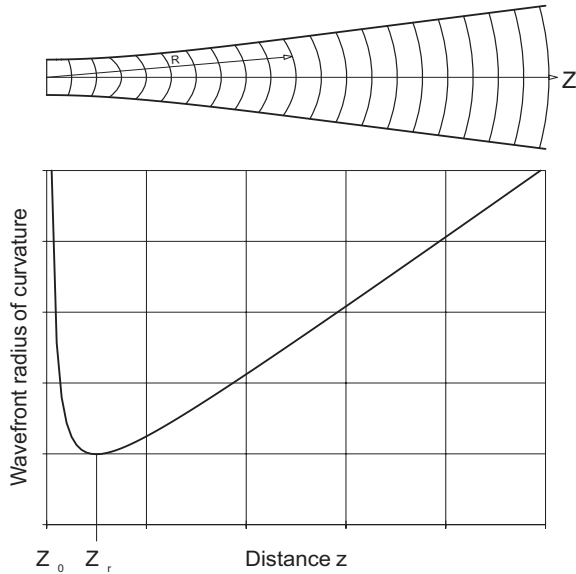


Fig. 30: The radius of curvature of a wave front as a function of the distance from the beam waist at z=0

The radius of curvature has a minimum at $z = z_r$ and R increases by $1/z$ compared to $z = 0$. The radius of curvature is infinite at $z=0$. The wave front is even at this point. The radius increases again linearly above the Rayleigh length z_r . This statement is of fundamental importance. It states that a parallel beam only exists at one point of a light wave, that is, in its focal point.

In the region for

$$z_r \leq z \leq z_r$$

a beam can be seen as approximately parallel or collinear. In Fig. 30 the Rayleigh area is drawn in as well as the divergence Θ in the far field region, i.e. $z \gg z_0$.

The graphic representations suggest that one of the significant characteristics of laser beams, i.e. their lack of divergence, cannot be shown in this way.

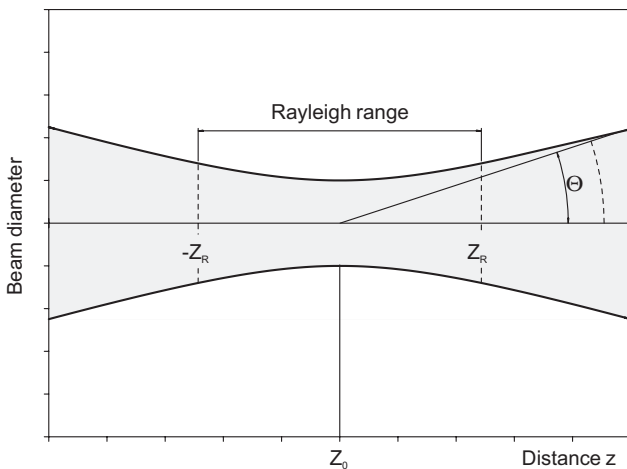


Fig. 31: Rayleigh range z_R and Divergence Θ in the far field region, i.e. $z \gg z_R$)

This is because the relationship of the beam diameter to z in the graphs has not been standardised. If we take a HeNe laser (632 nm) with a beam radius of $w_0 = 1\text{mm}$ at the exit of the laser as an example, we get:

$$2 \cdot z_R = 2w_0^2 \frac{\pi}{\lambda} = 2 \cdot 10^{-6} \frac{3.14}{623 \cdot 10^{-9}} = 9,9 \text{ m}$$

for the Rayleigh range $2z_r$. A moderate picture would therefore show only a thin line in the drawing.

1.10 Technical interferometers

In modern technical interferometers used in the calibration of CNC machines, the main light sources used are HeNe lasers. Modern CNC machines are positioned precisely at $1 \mu\text{m}$. Since this precision is dependent on the condition of the machines, a periodic calibration of the machines must follow. The measurement apparatus, the laser interferometer is supposed to be more precise than the test specimen according to Bernd's Law, i.e. it has a precision of $0.1 \mu\text{m}$. As we have already said previously and will be studying in more depth, it is possible to carry out resolutions into the nm area with laser interferometers. However, we have yet to establish the precision. We must first observe the errors for this purpose. If we want to reach the path S of the movable reflector M_2 through the number of light/dark transitions N , we must use the following equation

$$S = N \cdot \frac{\lambda}{\epsilon}$$

In this equation, λ is the wavelength of the light source used and ϵ is an integer scaling factor which had a value of 2 in the interferometer we have talked about till now. We must also keep in mind that the value of the wavelength λ depends on the refractive index n of the medium in which the wave expands.

$$S = N \cdot \frac{\lambda_0}{n} \cdot \frac{1}{\epsilon}$$

λ_0 is the wavelength in vacuum. If we use the total differential to determine the relative error of S , we will obtain:

$$\left| \frac{\partial S}{S} \right| = \left| \frac{\partial N}{N} \right| + \left| \frac{\partial \lambda_0}{\lambda_0} \right| + \left| \frac{\partial n}{n} \right| + \left| \frac{\partial \epsilon}{\epsilon} \right|$$

In a machine working range S of 1m the typical relative mechanical error of the machine will be $1\mu\text{m}/1\text{m} = 10^{-6}$. This means that the relative error of the laser interferometer for determining S should be smaller than 10^{-7}

$$\left| \frac{\partial S}{S} \right| \leq 10^{-7}!$$

The sum of the absolute values of individual error therefore has to be smaller than this value

$$\left| \frac{\partial N}{N} \right| + \left| \frac{\partial \lambda_0}{\lambda} \right| + \left| \frac{\partial n}{n} \right| + \left| \frac{\partial \epsilon}{\epsilon} \right| \leq 10^{-7}$$

Let us first consider the term

$$\left| \frac{\partial N}{N} \right|$$

The absolute error ΔN for determining a change from a dark to light fringe is $1/100$ of one counted fringe. There are $3,164,557$ fringe counts N for 1m resulting in

$$\left| \frac{\partial N}{N} \right| \approx \frac{0,01}{3.164.557} \approx 3 \cdot 10^{-9}$$

This is sufficiently precise. The errors formed through the variation in wavelength are:

$$\left| \frac{\partial \lambda_0}{\lambda} \right| = \frac{\partial \lambda}{0,632 \cdot 10^{-6}}$$

This leads to the demand that the absolute precision $\delta \lambda_0$ of the vacuum wavelength of the laser is smaller than 10^{-13} m or 10^{-7} μ m. The wavelength of a commonly used HeNe laser can fluctuate in a range of $1.5 \cdot 10^{-6}$. The laser will then have to be additionally stabilised for a measurement area of 1m. The term

$$\left| \frac{\partial n}{n} \right|$$

is caused by fluctuations in the refractive index caused by the surrounding air. The respective values of n are dependent on the air pressure, air temperature, the relative humidity and foreign gas in the surrounding air. The biggest influence on errors is caused by the variation in air pressure and in temperature. These values must be applied to reduce these errors and be taken into consideration in a correction calculation using the Edlen formula. The air pressure should be measured with an accuracy of 0.1 Torr and the temperature of 0.1° C, so as not to exceed the permitted errors. The final source for an error is the scaling factor e that is, however, a flawless constant in the apparatus. Modern HeNe laser with stabilised frequencies reach a precision of 10^{-9} . Apart from the type of stabilisation, all lasers have one disadvantage: Light cannot be reflected back into the laser. This is because the returning photons have another phase as those responsible for the stimulated emission in the laser resonator. Photons coming from outside would stimulate an emission which is not in phase with the basic oscillation of the resonator and can therefore stimulate undesired modes, which have a frequency other than the desired one. Because of this reason, the Michelson interferometer had to be modified so that no direct back coupling of light in the resonator would be possible.

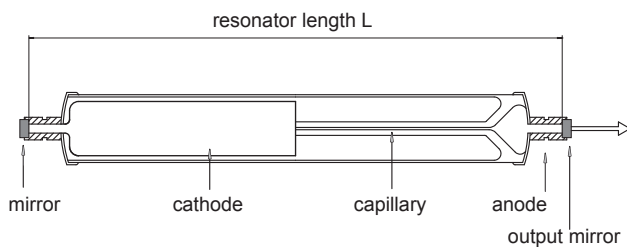


Fig. 32: Commonly used HeNe laser tube with mirrors soldered on to it with a distance of L.

The resonator length is approximately 130 mm for a single mode tube and 180 mm for a two-mode tube.

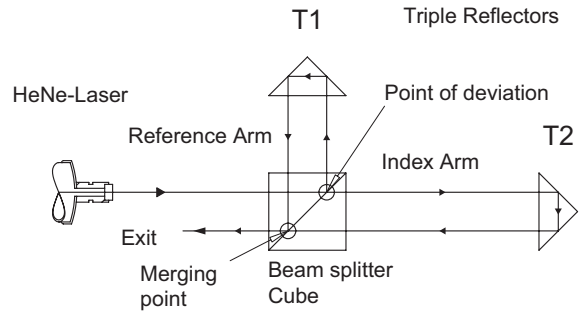


Fig. 33: Setup of a technical Laser Interferometer.

Instead of the beam splitter plate in the Michelson construction, a beam splitting prism is now used and instead of the plane mirrors, triple reflectors are used. This arrangement ensures that no radiation can return to the laser, contrary to the Michelson interferometer. The surfaces of optical components are also given anti-reflection layers to avoid return reflections from their surfaces. Polarising beam splitting prisms are usually used. The light in the reference arm is then vertically or orthogonal polarised with regard to the index arm. Before we discuss signal formation we will explain the structure and function of the optical components.

1.10.1 Beam splitting prism

The term beam splitting prism is used in common jargon. Actually a plate could also have been used instead of the prism. However, as shown in the following diagram, the plate has some disadvantages.

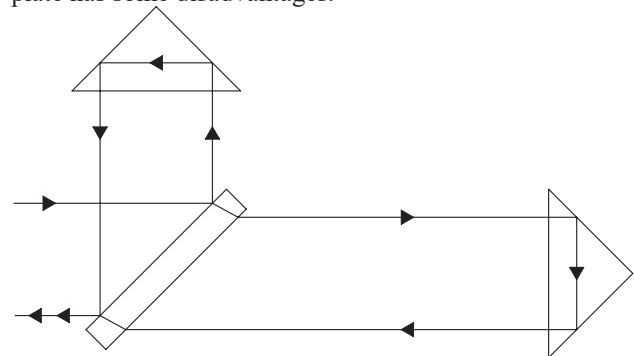


Fig. 34: Arrangement with a beam splitting plate

On one hand, there is a misalignment of beam for the sensitive index arm, which depends on the angle adjustment of the plate. On the other hand, the index beam crosses the plate twice. If the temperature of the plate changes, then its refractive index also changes considerably. This causes a phase shift that is interpreted as a movement of the triple reflector. The structure is not thermally compensated for.

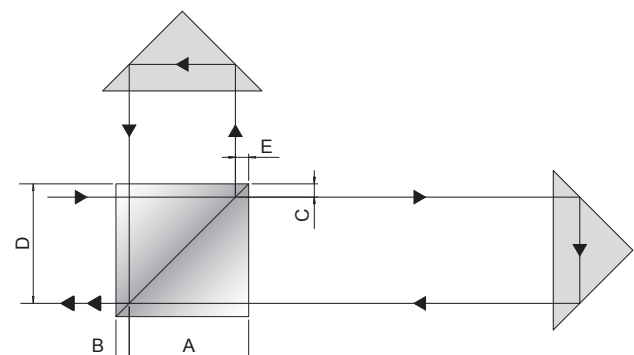


Fig. 35: Arrangement with a beam splitting prism

In this arrangement, the reference beam crosses the paths C+ triple reflector +D after the splitting point in the glass and up to the reunification point. The index beam crosses the paths E + triple reflector + A. These paths have the same length. A temperature change in the optical components therefore does not lead to a phase shift. The arrangement is compensated for thermally with regard to the optical components. Polarising beam splitting prisms are mainly used in technical laser interferometers that measure length. Contrary to neutral beam splitting prisms, the light is not split according to intensity, but is divided into orthogonal polarisation states.

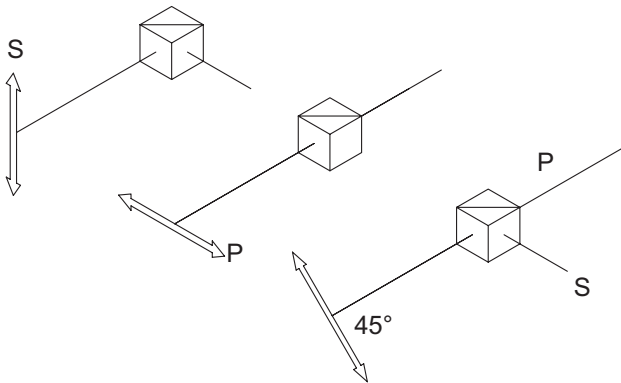


Fig. 36: Polarising beam splitting prisms

Vertically polarised light (S) is reflected on the inner layer of the prism, parallel light (P) is transmitted. If the polarisation direction of the light bends towards 45°, the beam splitting prism divides this light into its orthogonal components.

1.10.2 Triple reflector

If you cut a corner off a quadratic cube and put mirrors on the inner surfaces, you will get the important optical components of a triple reflector. Every light beam, which is led into the corner of this cube under any given angle, goes through three different reflections (A,B,C) and is finally reflected back into the same direction. There is, however, an offset between the incoming and outgoing beam, which is dependent on the place in the triple reflector onto which it falls.

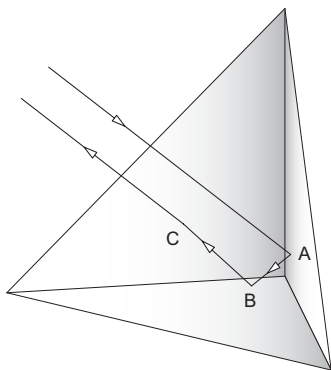


Fig. 37: Triple reflector

A corner can also be cut out of a cube made totally of glass. The reflection is then total reflection. This type of triple reflector is used most frequently. The advantage is, that the reflection surfaces are protected from dust and dirt.

1.10.3 Homodyne interferometer

The term homodyne interferometer was conceived at a time when heterodyne interferometers were in predominant use. The first commercial laser interferometer was patented and brought into the market about 25 years ago by Hewlett Packard. Other manufacturers because of the patent situation produced Homodyne interferometers. Today both types of systems are in usage. The light beam in the reference arm has a very different frequency to the light beam in the index arm. In this way the possibility of an alternating current coupled with gating is possible. The fluctuations in contrast are then of no significance. A detailed discussion will follow in the relevant chapter. The homodyne technique will be used for this experiment. This means that there is no frequency difference between the light in the index and reference arms. The structure is identical to Fig.32. However, special measures must be taken in detection so that the changing contrast does not influence consistent counting of the interference fringes. The following signal sequences are produced and evaluated for this purpose.

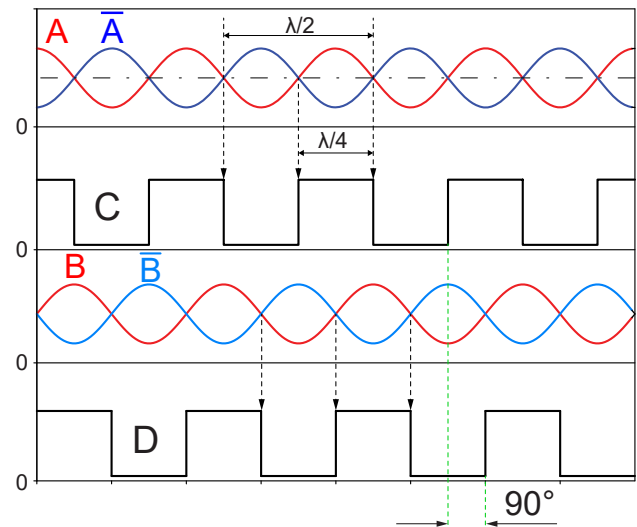


Fig. 38: Signal sequences required for safe counting of interference fringes.

The curves correspond to the equations

$$A \quad I = \frac{1}{2} E_{01}^2 + \frac{1}{2} E_{02}^2 + E_{01} E_{02} \cos(k \cdot \Delta L)$$

$$B \quad I = \frac{1}{2} E_{01}^2 + \frac{1}{2} E_{02}^2 - E_{01} E_{02} \cos(k \cdot \Delta L)$$

$$D \quad I = \frac{1}{2} E_{01}^2 + \frac{1}{2} E_{02}^2 + E_{01} E_{02} \sin(k \cdot \Delta L)$$

$$E \quad I = \frac{1}{2} E_{01}^2 + \frac{1}{2} E_{02}^2 - E_{01} E_{02} \sin(k \cdot \Delta L)$$

Curve A is the reference curve. Curve B is formed out of A through a phase shift of 180° and curve D is formed when curve A undergoes a phase shift of 90°. Curve E is formed when curve D goes through a phase shift of 180°. If we subtract curve B from curve A, the base is eliminated. The same is done with curves D and E. We can spare ourselves the subtraction work if we put the signals A and B, as well as E and D on a TTL-comparator. This type of comparator

has the following output characteristic:

$$\text{Output} = \begin{cases} \text{High if } A > B \\ \text{Low if } A < B \end{cases}$$

Signals C and F are produced in this way. Strictly speaking only counting the signal C is necessary, but we would then have no information on the direction in which the measurement reflector moves. The signal whose phase has been shifted by 90° has been produced for this purpose alone. The recognition of the direction happens in such a way that a toggle is dependent on the entrance at which a decreasing side is first detected. The exit signal from the toggle controls the following counter in the up or down mode. Let us make a timed observation of the signals C and F to understand this better. If the measurement reflector moves out of a condition at $z=0$ (Fig. 38) e.g. to the right, then the intensity at detector A increases and decreases at B. A is larger than B; the exit of the comparator is high. After some time $B>A$ and the corresponding comparator produces a decreasing side. The toggle sets the counter to up. If we were to go to the left from $z=0$ the first decreasing side would come from F and the toggle would be set back to enable the counter to switch to the Down mode. The necessary signals cannot be produced electronically. They therefore have to be provided by the interferometer.

1.10.4 Detection optics

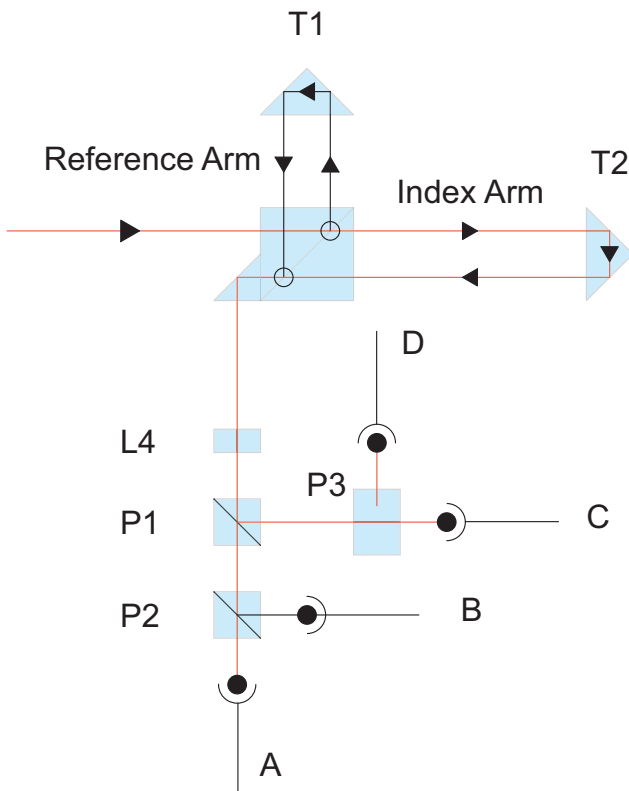


Fig. 39: Detection optics

By using a polarising beam splitter, the beams in the reference arm are polarised vertically to those in the index arm. It is well known that such polarising beams do not produce any interference pattern. They are sent through a small $\lambda/4$ plate (L4) to “persuade” them to make an interference pattern. This type of small plate consists of a birefringent crystal, e.g. natural quartz. This kind of crystal is not isotropic optically. Due to the natural crystal growth

it has two particular directions optically speaking that are caused by the asymmetry of the crystal cells. The inner structure of such a crystal can be compared to a forest of arranged antennae. An equal number of antennae receive both vertically and horizontally polarised radiation. These antennae are, in fact, dipoles that release the received radiation after a certain period of time. These dipoles take up a light wave entering the crystal one after the other and release it again. The two types of dipole also cause two different speeds of light in the crystal.

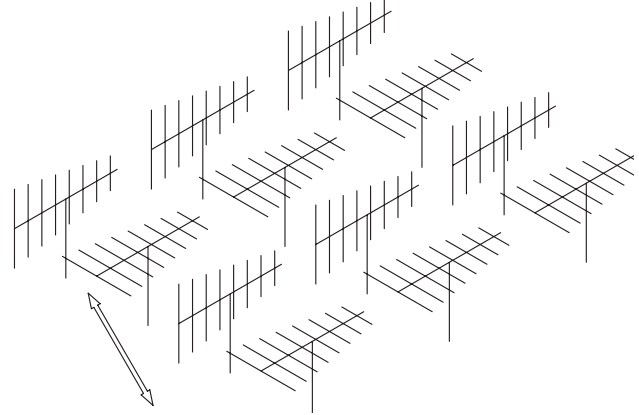


Fig. 40: Birefringent crystal as a certain number of orthogonal dipoles

If light with a polarisation of 45° is beamed into the “antennae forest”, the light intensity will be equally spread on the dipoles since the light with a polarisation of 45° can be interpreted as the superimposition of two orthogonal components.

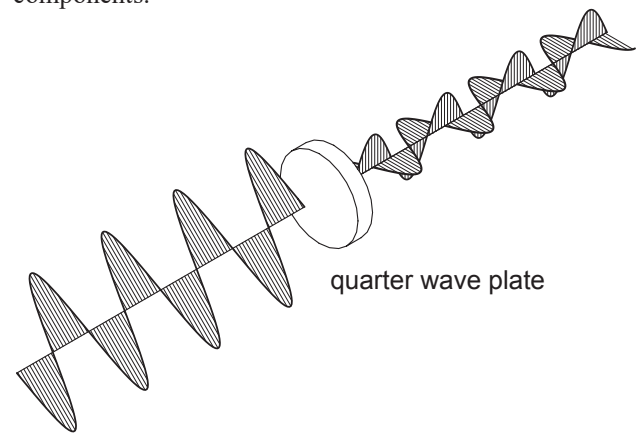


Fig. 41: Effect of a quarter-wave plate

At the exit of the crystal there is a phase shift between the S and P components, which is composed by the different speeds of the components in the crystal. If we select the number of antennae or the thickness of the crystal in such a way that this phase delay is just 90° or $\lambda/4$, then we obtain two merging waves which are vertically polarised towards one another and also have a phase shift of 90°. If we add up these field strength components vectorial, the resulting field strength vector will rotate with the frequency of the light beam on the axis of the direction of expansion. The light is now circularly polarised. Depending on whether the quarter-wave plate is reached under a beaming in angle of 45° or 135°, the polarised light will be right or left-handed circular. The quarter-wave plate sometimes has a mark on the edge that shows the direction “fast optical axis”. This axis is also described as the direction of the regular refractive index and the one at 90°, which is turned

at a certain angle to it, is called the “slow axis, also known as irregular refractive index.

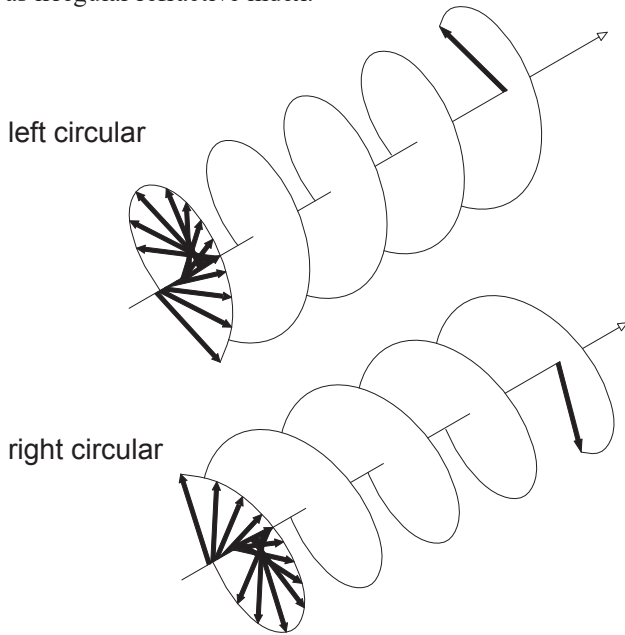


Fig. 42: Circular polarised light

Since we are sending two waves that are vertically polarised to each other from the interferometer into the crystal, we will obtain one left-handed and one right-handed circular wave behind the crystal. This can be shown more simply in the diagram of a circle.

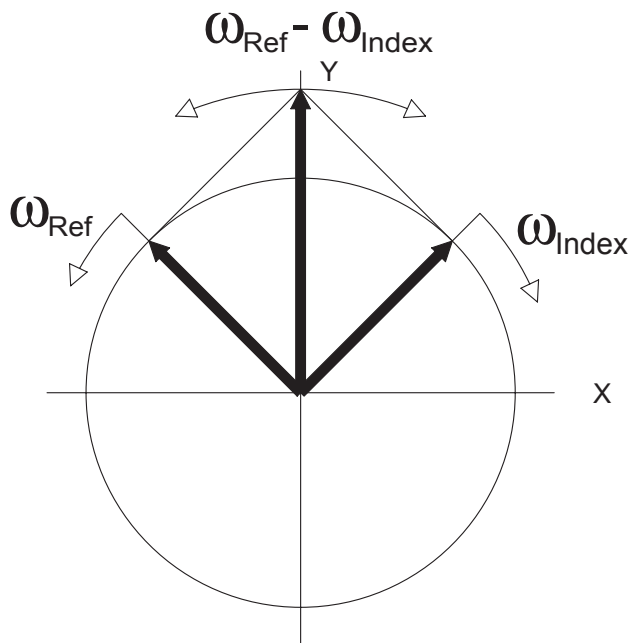


Fig. 43: Orthogonal circularly polarised waves and their resultants.

The above diagram shows a time exposure of the waves behind the quarter-wave plate. An indicator rotates at the frequency ω_{index} ; another one rotates in the opposite direction at a frequency ω_{ref} . If both frequencies are the same, the resulting indicator will be symmetrical to both the other ones and will only change its number. These changes happen so fast that a photodetector cannot follow them. If there is a difference in frequency between the beams coming from the index and reference arms, the resulting indicator starts to rotate with the frequency of the differ-

ence. The direction of rotation depends on the signs indicating the difference. If we allow this light to pass through a polariser, a photodetector will detect a signal which has been temporally changed and which coincides exactly with the frequency difference. But what is the reason for this frequency difference between the reference and index beam? As long as the measurement reflector is not used, both frequencies are the same. If, however, the measurement reflector moves, the light frequency changes due to the Doppler effect. This happens according to:

$$\omega_{Me\beta} = \omega_0 \cdot \left(1 \pm \frac{2 \cdot v}{c} \right) \quad \omega_{Ref} = \omega_0$$

In this case ω_0 is the frequency of the laser, v is the speed of the measurement reflector and c the speed of light. Factor 2 of the speed moves, because the beam length is changed by 4 cm, when, for example, 2cm is shifted due to the double passage of the light in the index arm. The difference in frequency is therefore:

$$\Delta\omega = \omega_{Ref} - \omega_{Me\beta} = \mp \omega_0 \frac{2 \cdot v}{c}$$

We will not use the sign \pm just now. The following are also used:

$$\Delta\omega \cdot \frac{c}{2 \cdot \omega_0} = \frac{dz}{dt}$$

or

$$dz = \frac{c}{2\omega_0} \cdot \Delta\omega \cdot dt$$

$$\int_{z_1}^{z_2} dz = \frac{c}{2\omega_0} \cdot \int_{t_1}^{t_2} \Delta\omega \cdot dt = \frac{\lambda_0}{2} \cdot \int_{t_1}^{t_2} \Delta\nu \cdot dt$$

If we therefore take into consideration that $\Delta\nu$ is the number ΔN of the rotations of the resulting indicator per time unit counted by a counter, then

$$\Delta\nu = \frac{\Delta N}{dt}$$

$$s = z_2 - z_1 = \frac{\lambda_0}{2} \cdot \int_{t_1}^{t_2} \frac{\Delta N}{dt} \cdot dt = \frac{\lambda_0}{2} \cdot N$$

The result is therefore the same as in the simple Michelson interferometer. The reason why this method is used is because it is now possible to split up the resulting beam and to send it through differently oriented polariser. Let us return to Fig. 38 where we can see in the optical structure that both the orthogonal circularly polarised waves meet after the quarter-wave plate (L4) on the neutral beam splitter (P1) and are split into two channels at that point. One part of the radiation reaches the polarising beam splitting prism P2. This fulfils two tasks. On one hand it splits the radiation and on the other hand it is effective as a polarising analyser. The phases of the signals A and B are then shifted towards each other by 180° , as desired. The polarising beam splitter (P3) is arranged at a 45° angle in the second channel, so this channel has a phase shift of 90° compared to the other channel. The phases of the signals C and D are again shifted towards each other by 180° . In this way we obtain the necessary phase shifts to compensate

the varying contrast on one hand, and to obtain signals for the forward/reverse recognition on the other hand. The difference between the Michelson interferometer and this method is, that we do not obtain the path information from a contrasting picture dependent on location, but from the fluctuation or mixture of two optical frequencies. Since we use only one basic frequency for the mixing process, i.e. the frequency of light, this process is also called the homodyne process.

but the electronic preparation would be more expensive. Nowadays both interferometers have an equal place in the market and both perform with the high precision required.

1.10.5 Heterodyne interferometer

An optical intermediate frequency is used in this process. It is obtained mainly from the frequency interval between the modes of a laser.

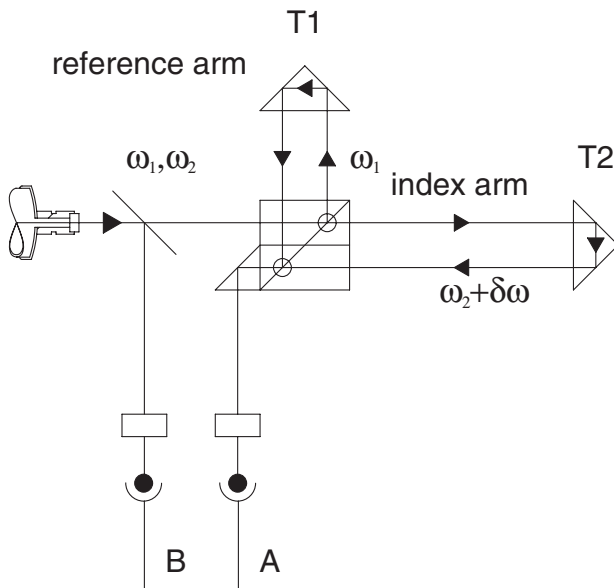


Fig. 44: Heterodyne interferometer

This frequency difference is approx. 2MHz in the case of older equipment. It is produced when a single mode HeNe laser tube is surrounded by a longitudinal magnetic field. The mode splits into two circularly polarised modes due to the Zeeman effect. The size of the slit and the frequency difference depends on the magnetic field strength. After both circular modes have crossed a quarter-wave plate, the modes that are now orthogonal are sent into the interferometer, which would otherwise have the same optical structure.

A polarisation filter is placed in front of detector B, which detects the frequency

$$\omega_1 - \omega_2$$

Detector A sees the frequency

$$\omega_1 - \omega_2 \pm \delta\omega$$

In this case $\delta\omega$ is the change in frequency that is produced by the Doppler effect or by the movement of the measurement reflector. Both signals are electronically mixed, subtracted from each other and carried out using a phase discriminator, which carries out forward-reverse recognition. Since both detector A and detector B only “see” alternating stress signals, fluctuations in the contrast are already eliminated. Optical detection is obviously easier

2. Experiments

2.1 Michelson Interferometer

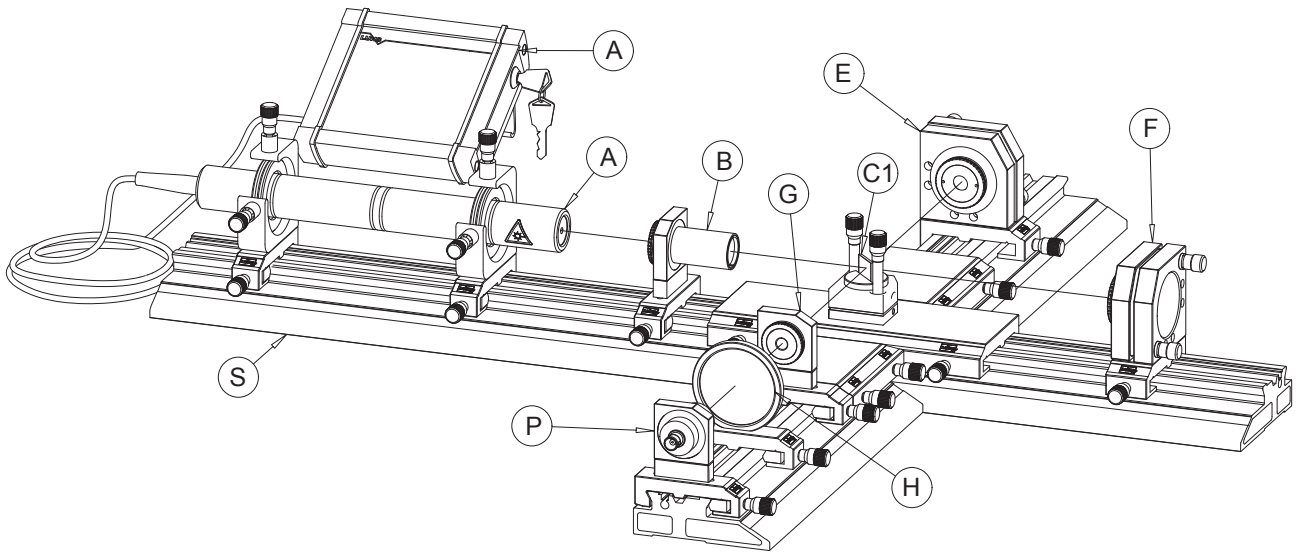


Fig. 45: Set-up of the Michelson Interferometer showing the modules

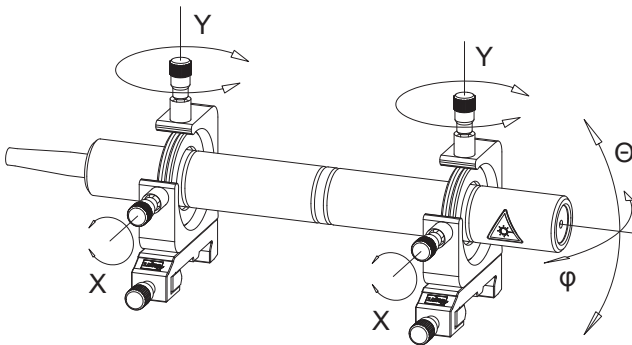


Fig. 46: Module A, HeNe-Laser

The HeNe-laser is a two-mode laser with a frequency difference of 900 MHz between both orthogonal modes, which are randomly polarised. This means, that although both modes are linearly polarised the direction of the polarisation depends on the tube geometry. The direction is defined by anisotropisms of the capillary diameter and by low birefringence of the dielectric coated mirrors. The laser tube can be turned in its holding device for adjustment to the desired polarisation direction. The beam diameter is 0.5 mm at the exit and the divergence is 1.5 mrad. The output power is at least a maximum of 2.5 mW. This type of laser for the beam that is not expanded belongs to the laser safety class 3b, whereas beams after the telescope come into the category 3a because of the reduction in intensity.

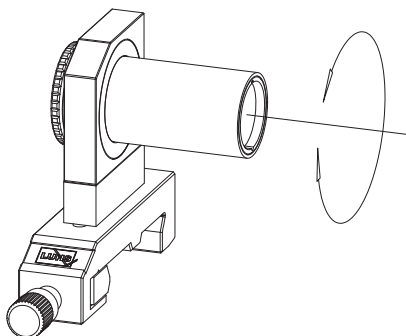


Fig. 47: Module B: Beam expander

The beam is expanded eightfold with this telescope and serves the purpose of reducing the divergence thus resulting in more plain wave fronts. The telescope is adjustable and the divergence of the expanded beam can therefore be changed to produce, for example, also curved wave fronts.

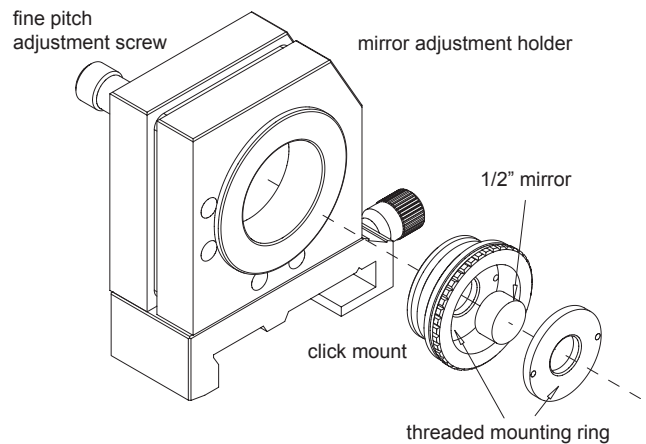


Fig. 48: Module E Mirror M1

A mirror adjustment holder carries the flat mirror M1 that is inserted into a click-stop mount and fixed by means of a threaded mounting ring. The entire click mount assembly can therefore simply be “clicked” into the adjustment holder where it is kept in position by spring-loaded balls. With high precision fine pitch screws the mirror can be tilted in two orthogonal axes with respect to the optical axis. The mirror has a diameter of $\frac{1}{2}$ inch, a thickness of $\frac{1}{4}$ inch and flatness of $\lambda/10$. One side is coated with a high reflective layer ($>99.98\%$).

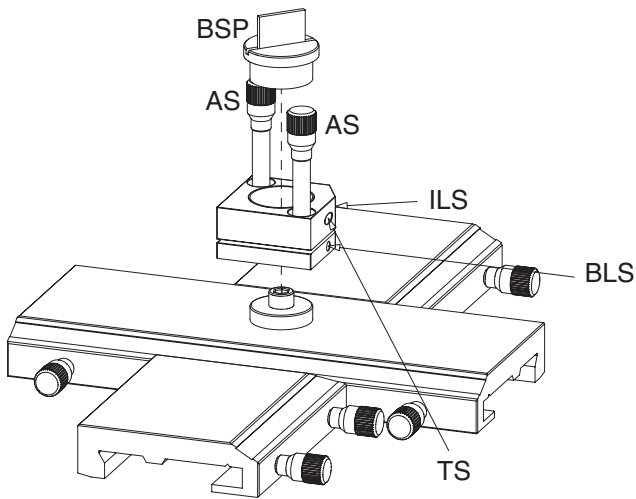


Fig. 49: Module C1: Beam splitter assembly

The beam splitting plate is mounted in a holder (BSP) and divides the incoming beam at a ratio of 1:1. The mount is inserted into the adjustment holder and fixed by the lock screw (ILS) and can be turned around its vertically axis by turning the screw (TS). For this purpose an Allan key screwdriver is provided. By means of the two adjustment screws (AS) the beam splitting plate can be tilted. The adjustment holder is fixed by means of the lock screw (BLS) to the crossed carrier.

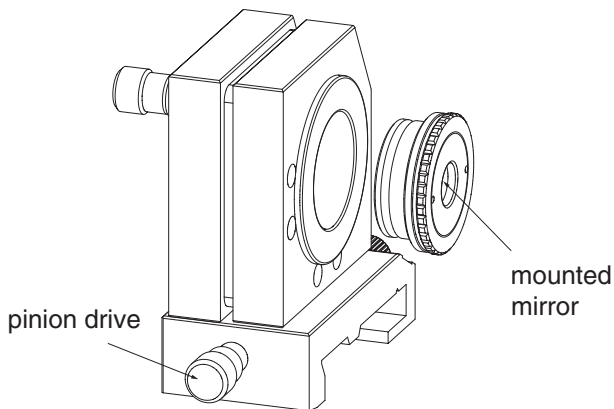


Fig. 50: Module F: Mirror M2

The mirror M2 has the same click mount as well as specifications as mirror M1 and is mounted into a same adjustment holder. However, its carrier is supplied with a pinion drive, which in connection with the gear that is integrated into the rail allows the forth and back movement of the entire assembly on the optical rail.

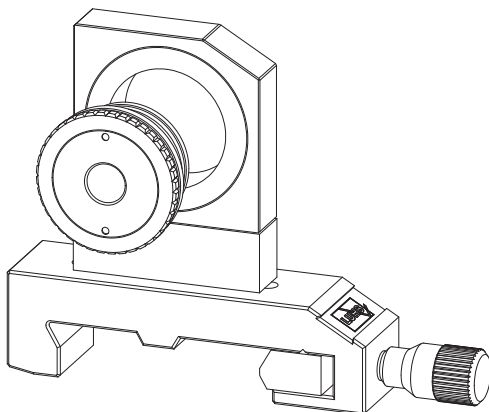


Fig. 51: Module G Beam expander

A concave lens with a short focal length of -10 mm expands the interfering beams. In this way they appear larger on the screen (Module H).

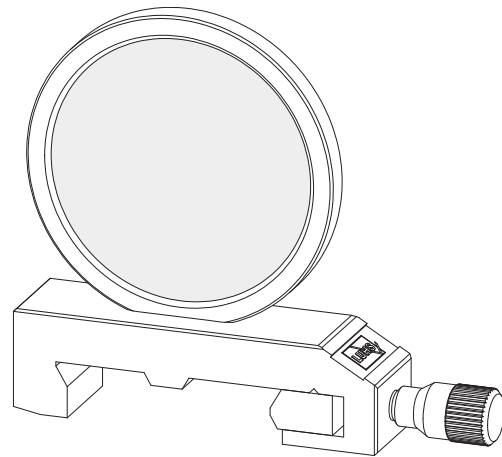


Fig. 52: Module H optical screen

The screen is supplied with exchangeable parchment paper for displaying the interference pattern.

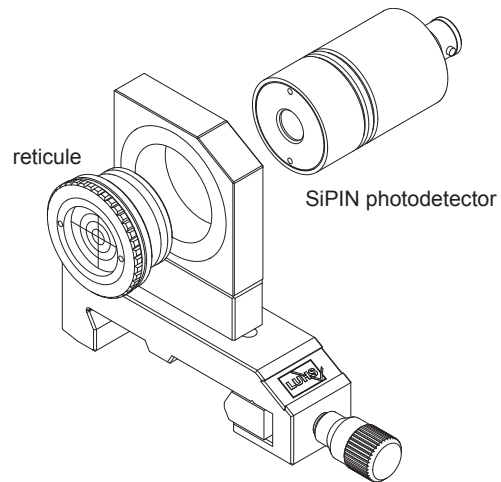


Fig. 53: Module P: Photodetector

A Si PIN photodiode (BPX61) is built into a housing supplied with the click mechanism for easy snap-in to the mounting plate. The signal of the photodiode is available at the BNC socket and can be connected to an oscilloscope to display the interference fringes. The module is further equipped with a crossed hair target mounted in a click holder and serves as an alignment aid of the set-up

2.1.1 Adjustment of the Michelson Interferometer Step 1

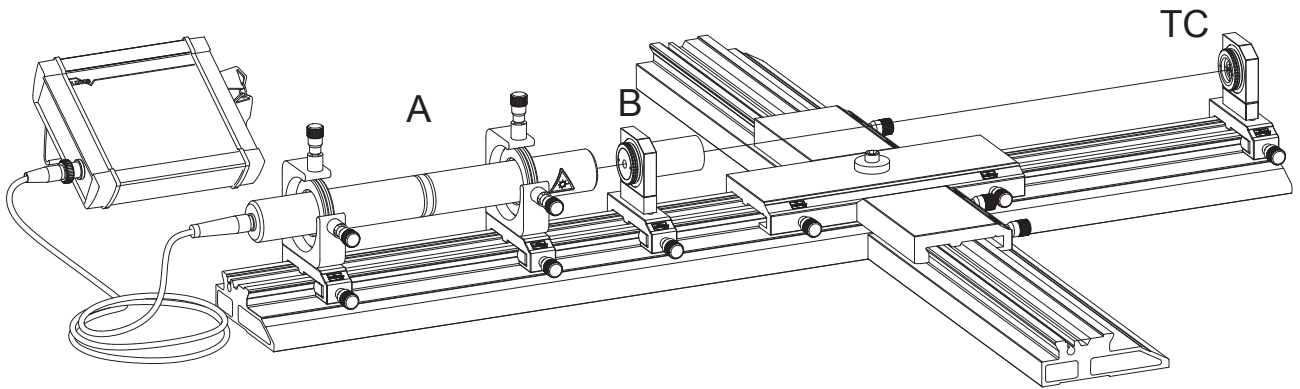


Fig. 54: First step

The first step is to remove all components except the HeNe-laser (A) and the telescope (B). The mounting plate with inserted crossed line target (TC) is placed on the rail. Adjustment can now take place using the XY fine adjustment screw of the HeNe-laser holder up to the time an

undisturbed circular centred laser patch can be seen on the target. A sheet of paper is used to test if the beam is actually parallel along its path. If not, the divergence is adjusted by turning the exit lens of the telescope.

2.1.2 Alignment Step 2

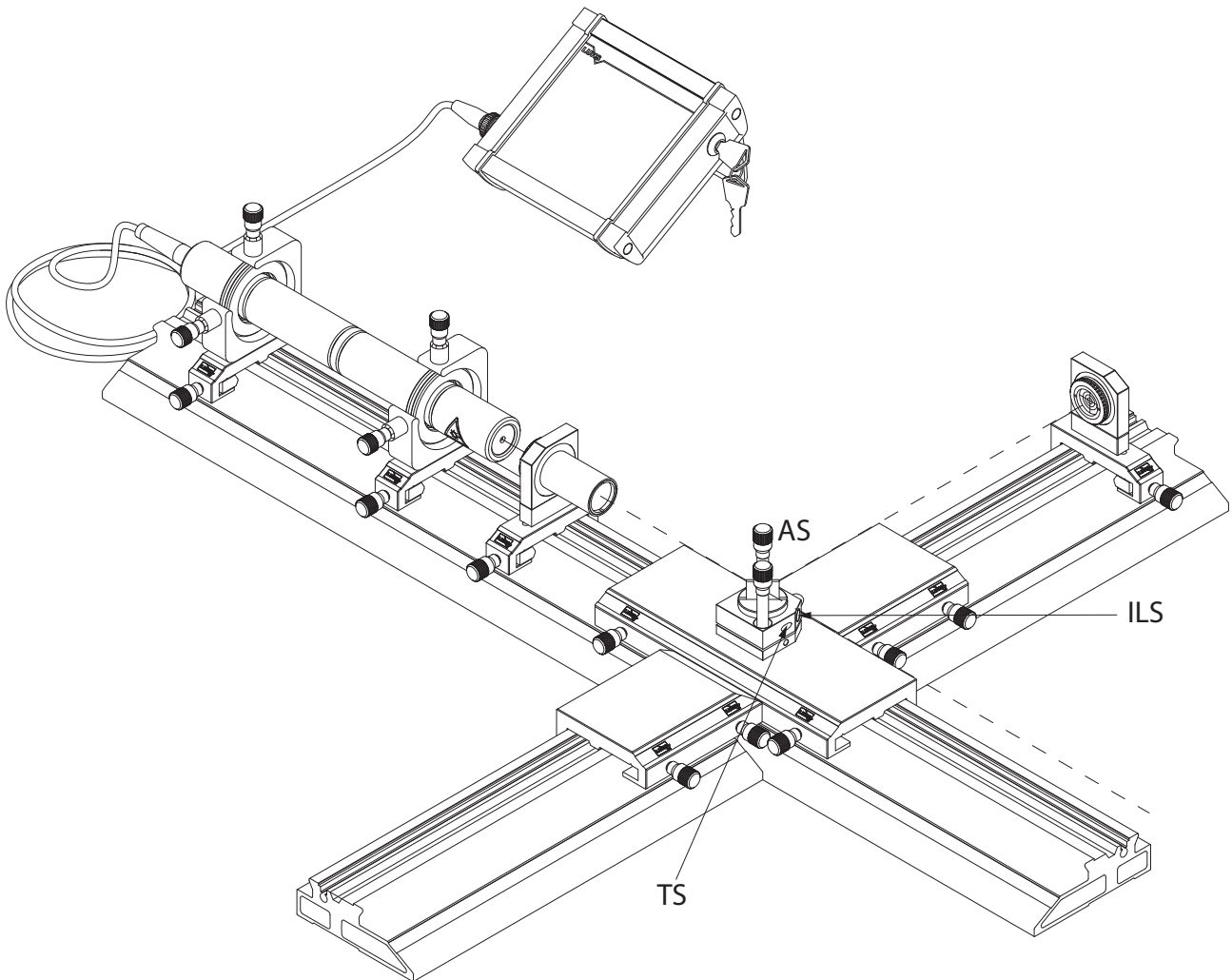


Fig. 55: Second step

After inserting and fixing the holder with the beam splitting plate, the diverged beam is adjusted with respect to the optical axis of the reference arm using the target. To do this, the beam splitting plate holder is coarsely turned and subsequently fixed (ILS). For fine-tuning the insert is rotated by turning the adjustment screw (TS). Deviations

in height are adjusted with the adjustment screws AS.

Step 3, alignment of the mirrors

2.1.3 Step 3, alignment of the mirrors

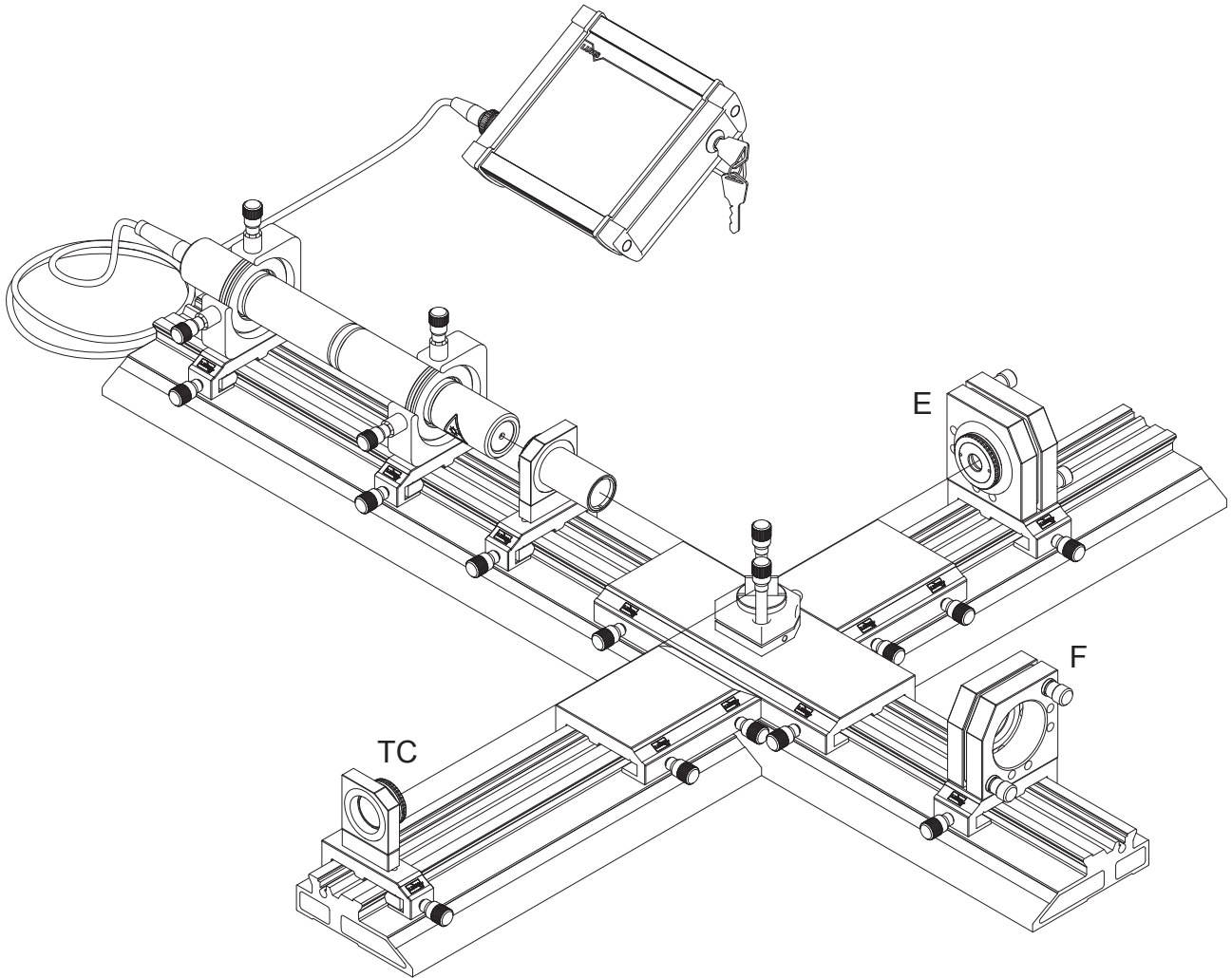


Fig. 56: Step 3, inserting the mirrors E and F

First, a mirror adjustment holder (E or F) with the plane mirror is placed on the rail. The beam that reflects back is adjusted with the fine adjustment screw of the adjustment holder in such a way that it touches the centre of the target screen (TC). Now the next mirror adjustment holder is placed on the rail. The reflected beam of the previous mirror is blocked out using a sheet of paper and the adjustment of the second beam can then be done with a better perspec-

tive. Now the target cross is removed and the beams are tested as to whether they still merge with a larger distance. If both beams are well adjusted to each other we will already be able to observe a variation in intensity. The first interferences!

2.1.4 Interference patterns

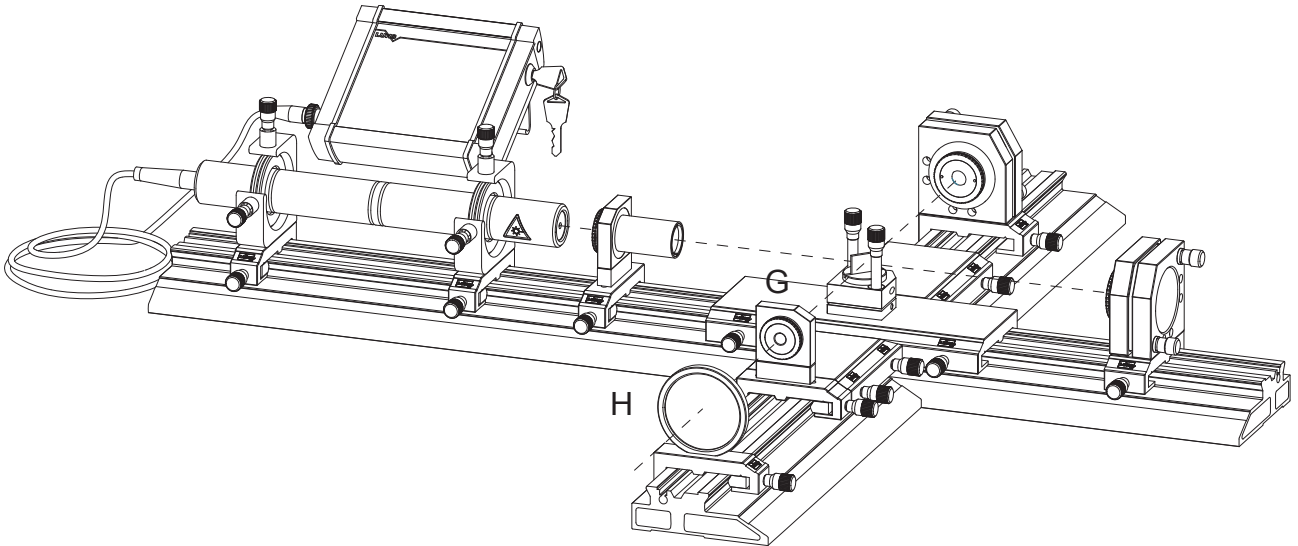
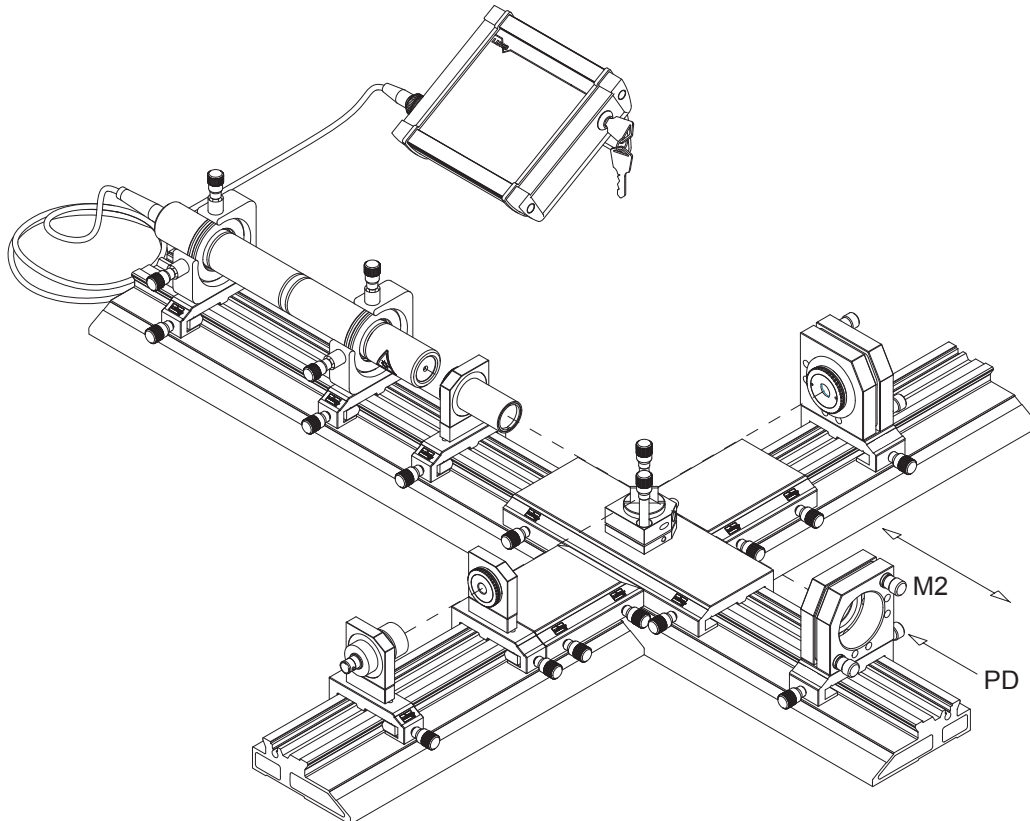


Fig. 57: Displaying the interference Pattern

The beam expander (G) and the screen (H) are now placed on the rail. You will now observe interference patterns on the screen. If you touch the structure at any point, the interference pattern will wander correspondingly. The size of the image can be selected by changing the distance between beam expander (G) and the screen (H). Different

interference patterns with varying contrast or structure can be realised by further adjustment. By changing the divergence of the laser beam, circular pattern can also be formed instead of stripes. After changing the divergence there should be some further adjustment.

2.1.5 Measuring the contrast function $V(\delta L)$



For this measurement the screen will be replaced by the photodetector. The distance is chosen in such a way that just one fringe (light or dark) covers the sensitive area of the detector. The Interferometer is now tuned to its zero order. This means the path difference of the reference arm is equal to the index arm. The detector is directly coupled

to an oscilloscope (a storage scope will be very convenient). If one now moves mirror M2 a little bit by turning the pinion drive screw (PD) the interferogram at this position of M2 will be shown on the oscilloscope. The contrast is determined for this position. This will be continued until the contrast reaches its minimum.

2.2 Technical interferometer

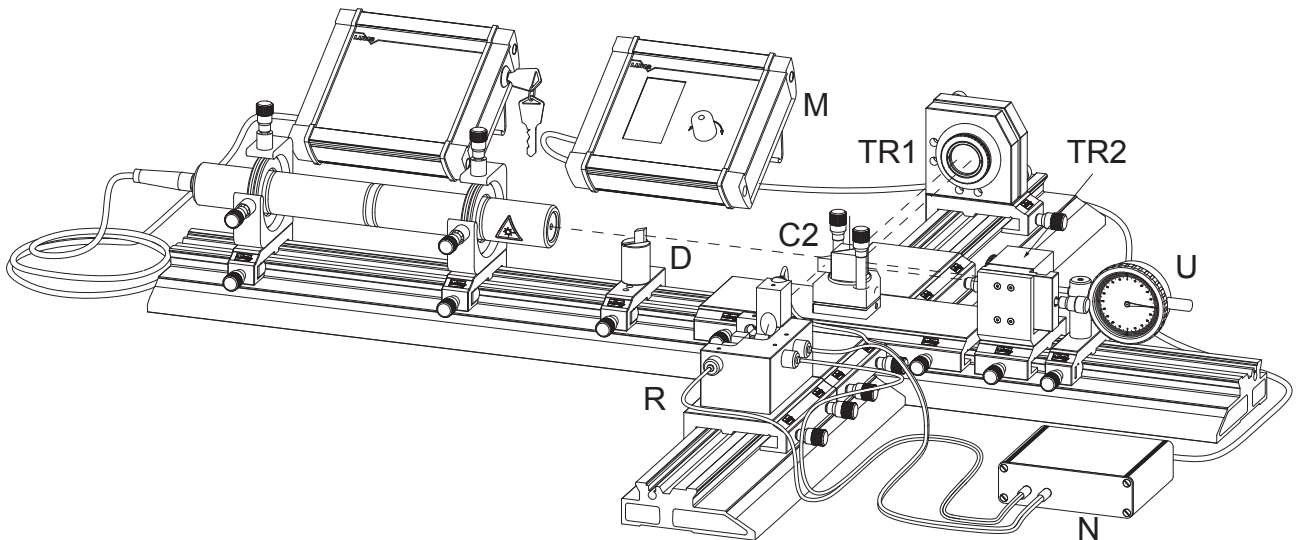


Fig. 58: Fig. 2.6: Set-up of technical Laser Interferometer showing the additional modules

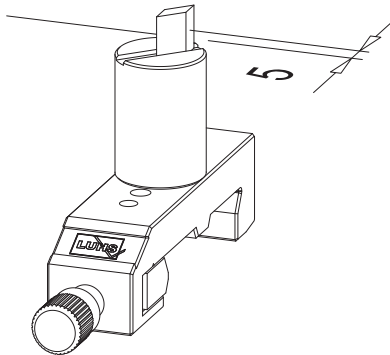


Fig. 59: Module D: Beam bender

A glass prism is used to obtain the required parallel beam offset of 5 mm with respect to the optical axis of the interferometer.

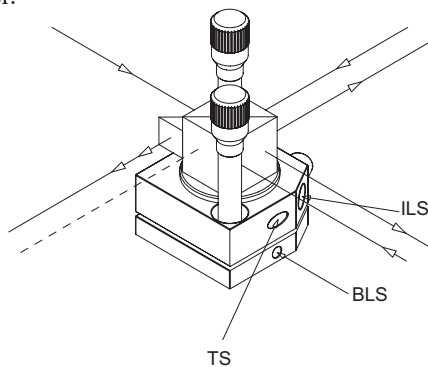


Fig. 60: Module C2: Beam splitting and combining assembly

The laser beam coming from the module D (beam bender) enters the polarising beam splitting cube where it is divided into two beams. One beam leaves to the triple reflector T1 and the other to T2. From both they are reflected back with a parallel offset of 10 mm and entering the polarising beam splitting cube again where they are recombined in such a way that they are travelling each inside the other. Both beams exit through the diverging prism and now have to be merged perfectly together. Horizontal deviations are balanced out by turning the beam splitter holder (TS), whereas vertical deviations are corrected using the adjustment screw. Apart from the main beam, we can observe another one (broken line), which is formed by parasite ef-

fects. This is because the absolutely pure polarisation and separation cannot be reached in practice. Contrary to the Michelson interferometer, there are no intensity fluctuations due to interference in spite of a flawless adjustment. This is because both beams are polarised orthogonal to each other. To generate the required intensity variation due to interference as well as 90° and 180° phase shifted signals for the further signal processing and direction discrimination the detection unit module R is used.

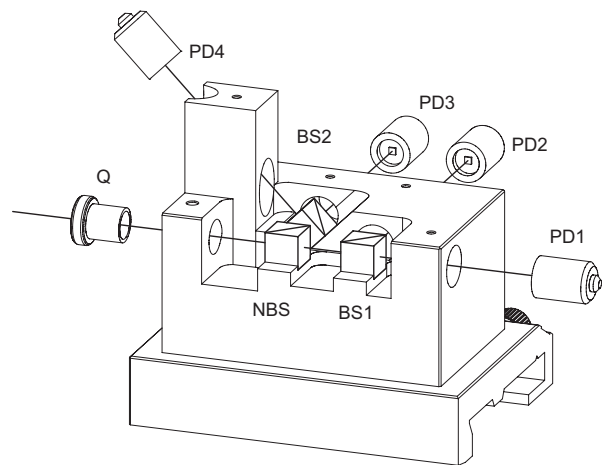


Fig. 61: Module R: Fringe detection unit

The two beams merged to one beam leaving the bending prism of the beam splitting and recombining module C2 are entering the detection unit via a quarter wave plate (Q) where their linear orthogonal polarised state is converted to a circular one. A fraction of 50% is reflected by means of the neutral beam splitting cube (NBS) to the polarising beam splitter BS2 and the other fraction is transmitted to BS1. As a result both fractions are now phase shifted of 180° to each other. BS1 again divides the beam into two fractions of equal intensity, which have a phase shift of 180° to each other and are detected by the photodiodes PD1 and PD2. The same happens at BS2 however; the cube is turned by 45° with respect to BS1 resulting in an optical phase shift of 90° to the beams leaving BS1. Detector PD1 sees the in phase signal, which we term as \sin . Consequently at PD2 a $-\sin$, at PD3 a cosine and at PD4 a $-\cos$ signal will be present.

Measuring the contrast function $V(\delta L)$

All four signals will be amplified and processed in the preamplifier PDA-01 (module N).

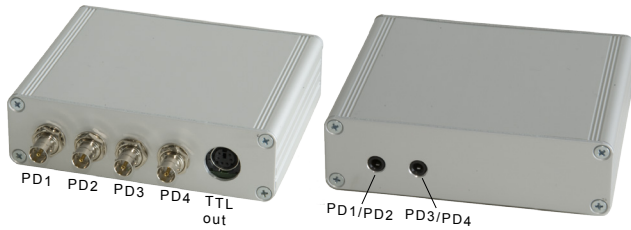


Fig. 62: Module N: Preamplifier PDA

The preamplifier has two functions. Firstly it amplifies the four photo diode signals and secondly it generates by means of a comparator TTL signals, which can be counted by the subsequent counter module M. The output signal A of the PDA-01 is formed by the first comparator fed by the PD1 and PD2 signals and B by the second one fed by PD3 and PD4. The TTL signals A and B, which have a phase shift of 90° to each other, are used to discriminate forward or backward movements of the triple reflector. These signals are available on the two mini BNC exit sockets of the counter and often termed as quadrature signals.

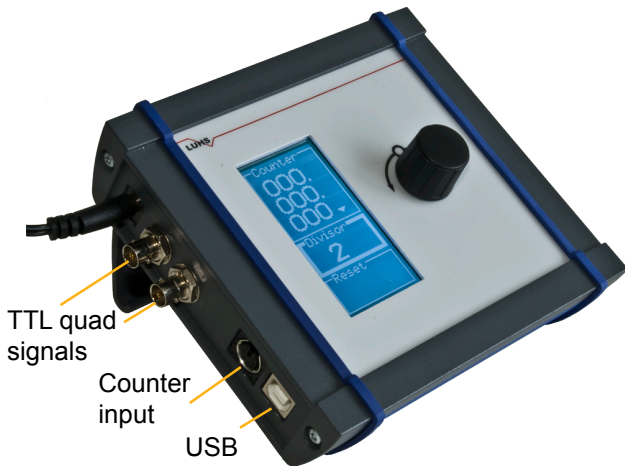


Fig. 63: Module M: Up and down counter FC-01

The counter FC-01 receives the signals A and B from the preamplifier module N. Depending on which falling edge of the TTL signal of A or B occurs first, the direction of count either up or down is defined. By exploiting the rising and falling edge of the TTL signals A and B an interpolation can be realised, resulting in a resolution enhancement of factor 2 or 4. Without interpolation one count event relates to a movement of the triple reflector of $\lambda/2$. By using the internal interpolation a movement of $\lambda/4$ or $\lambda/8$ corresponds to one count event. To calculate the movement the displayed result must be multiplied by the wavelength $\lambda = 0.632 \text{ nm}$ and divided by the interpolation factor used. The counter FC-01 is controlled by a microprocessor. The settings are done by a one button control which navigates through the available menu. Via the USB bus the measurement results can be transferred to a computer. In addition the counter can be fully controlled by a connected computer.

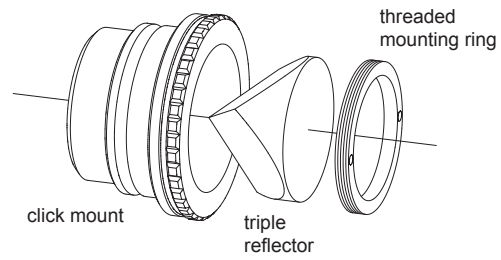


Fig. 64: Module TR1: Triple reflector

The triple reflector TR1 is mounted into a same housing with click mechanism as the mirror M1 or M2 and therefore M1 will be replaced by TR1 whereas the reflector TR2 builds it own unit containing a translation stage to perform linear movement with respect to the optical axis of the interferometer.

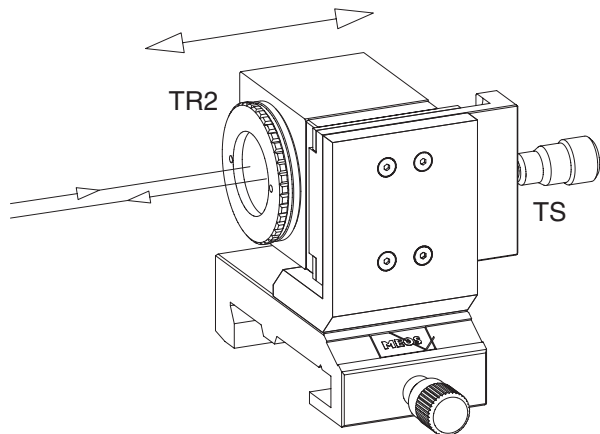


Fig. 65: Module TR2: Triple reflector with translation stage

The triple reflector TR2 is mounted into a block, which is fixed to a translation stage (TS) allowing the movement with in arrange of 5 mm. By turning the micrometer screw with a pitch of 0.25 mm per turn the reflector is moved into the desired direction. At the backside of the block containing the reflector TR2, a steel plate is supplied, where the steel ball tip /TI) of the micrometer dial gauge of module U butts against it to measure the movement with a resolution of $1 \mu\text{m}$.

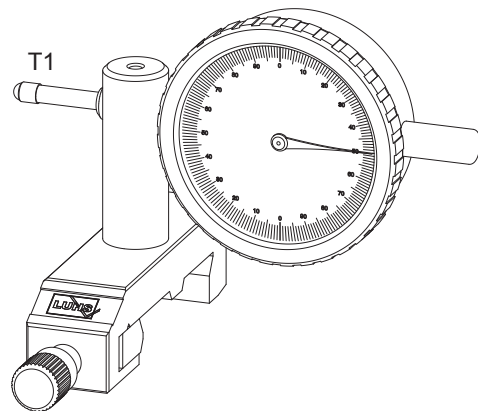


Fig. 66: Module U: Micrometer dial gauge

2.2.1 Set-up of Technical Interferometer step 1

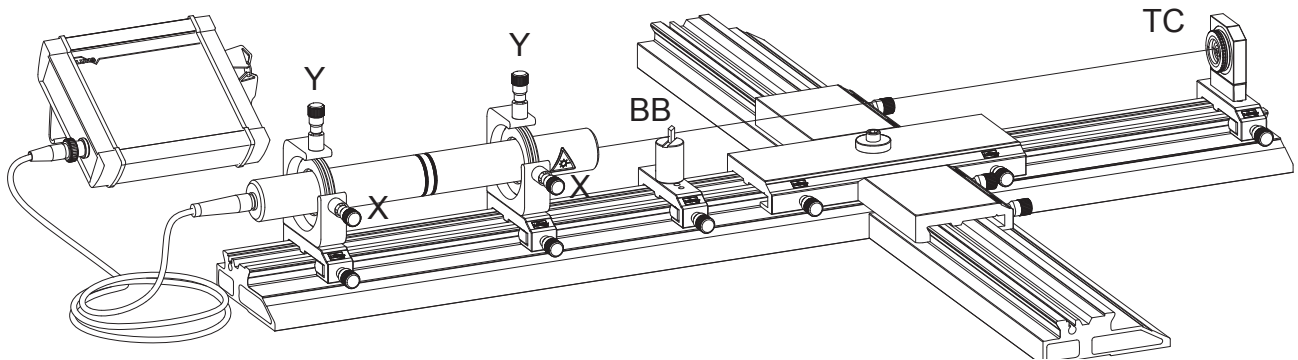


Fig. 67: Fig. 2.7: Using the beam bender and aligning the beam

Remove all modules except those ones as shown in the figure above. Place the hair crossed target (TC) at the end of the rail and align the beam by adjusting the HeNe-Laser tube in such a way that the beam hits the target with a lateral offset of 5 mm. Check this also for other positions of the target on the rail.

2.2.2 Set-up of the beam splitting and recombining module

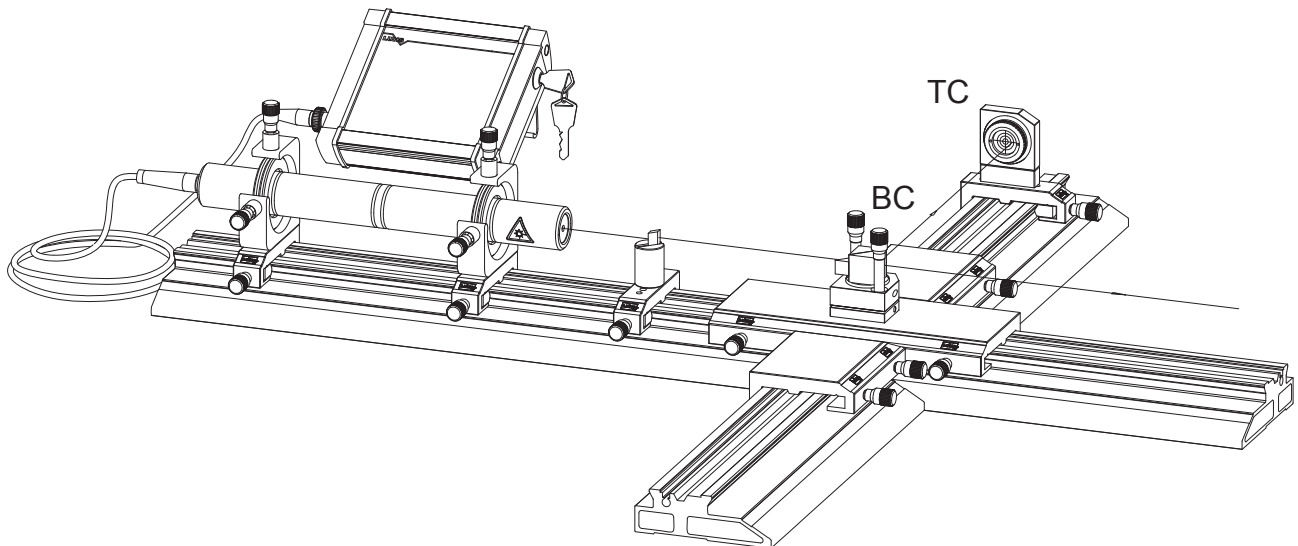


Fig. 68: Fig. 2.8: Alignment of the beam splitting unit

In the next step the beam splitting and recombining module BC is attached and fixed to the cross piece carrier. Place the target screen (TC) nearly at the end of the reference arm and turn the insert with the beam splitting cube in such a way that the beam hits the target screen with a horizontal offset to the right from the centre of 5 mm. Check this also for other positions of the target screen on the reference arm.

2.2.3 Set-up of triple reflector TR1 and TR2

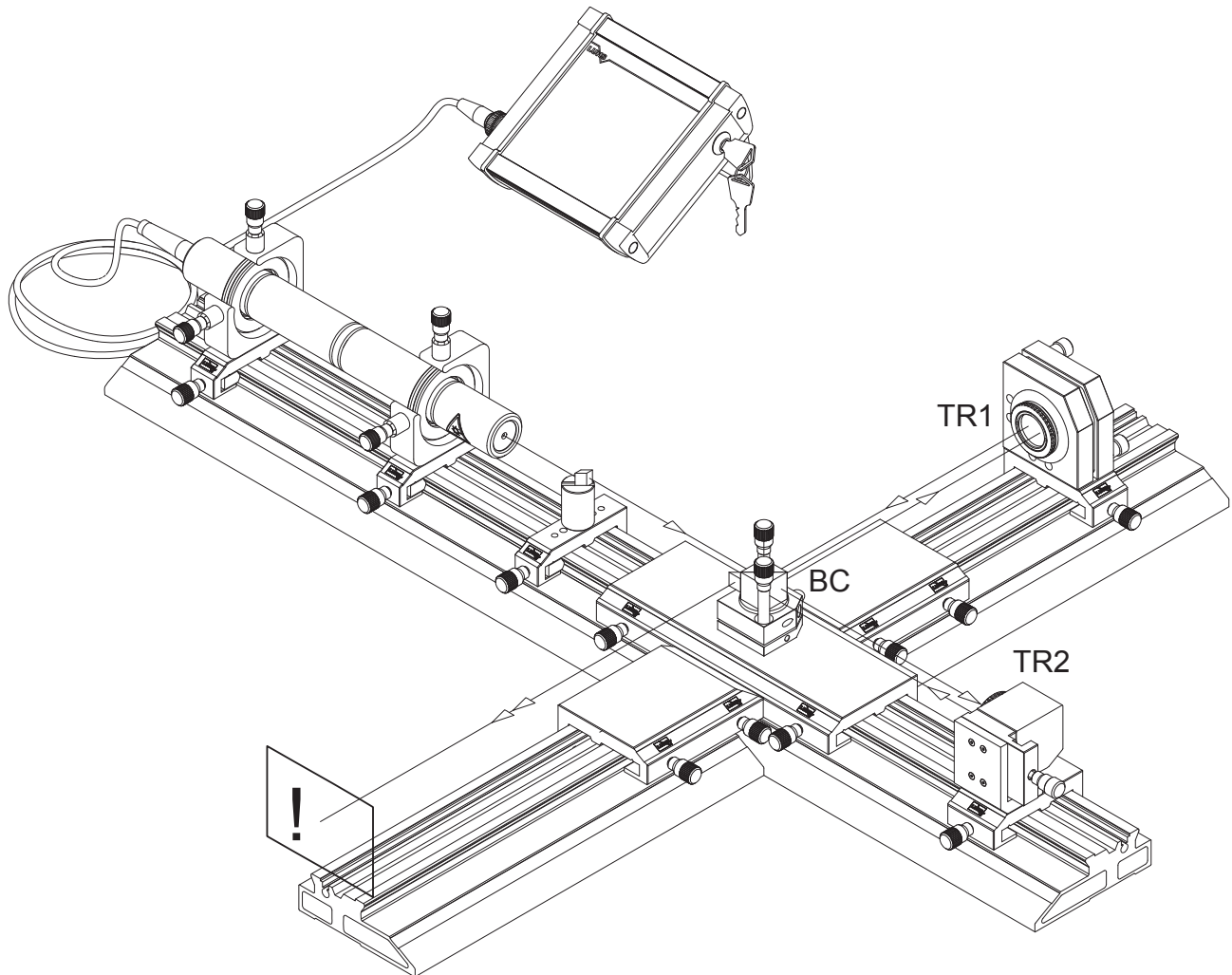
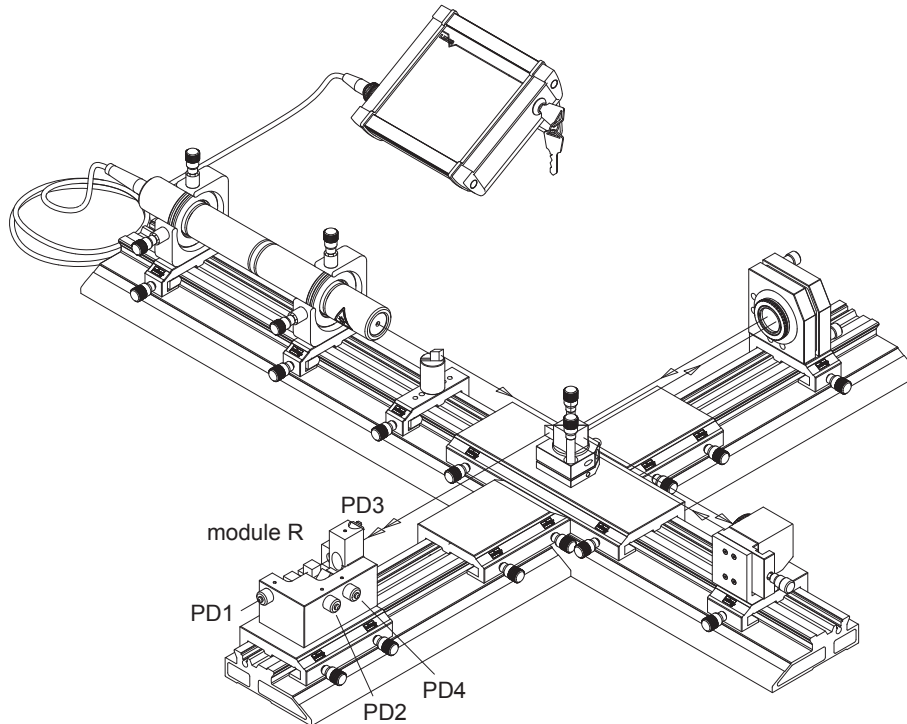


Fig. 69: Fig. 2.9: Inserting the triple reflector T1 and T2

Now the triple reflector TR1 is inserted into the mirror adjustment holder and placed on the rails, after that the moveable reflector TR2 is placed on the rail. 10 mm apart from the incoming beam the reflected beam leaves the triple reflector and travels to the beam-recombining cube of BC where both beams are merged to one beam. To check if

both beams are really merged to one circular beam, use a sheet of white paper at a location indicated by the exclamation mark of the figure above. Block the beam of TR2 to observe the beam of TR1 only and vice versa. If necessary realign BC as well as the laser tube.

2.2.4 Set-up of the signal detection unit



2.2.5 Signal detection

After the beams have been adjusted, the optical detection unit (module R) is placed on the rail. Cables are led from Detectors PD1, PD2 as well as PD3 and PD4. The sine and cosine definitions can be chosen freely. The plugs are connected to the sockets on the front side of the pre-amplifier PDA-01. The amplified interferometer signals are then available on the BNC sockets and can be connected to an oscilloscope. For fine-tuning the interferometer, the exit signals of the preamplifier must be observed on a two-channel oscilloscope.

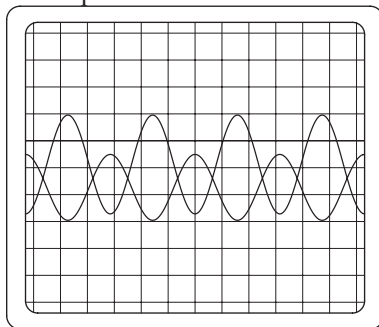


Fig. 70: Display of proper aligned interferometer

The adjustment has been done properly if the image is as shown above. There are a total of four possibilities for fine-tuning:

1. The orientation of the laser regarding its axis (direction of polarisation)
2. Rotation of the triple reflectors in their frames. A turn in polarisation takes place due to the total reflection on the inner surfaces of the edges of the cube. This can be minimised.

Rotation of the quarter-wave plate. The plate should be under 45° to both orthogonal light beams.

3. Adjustment of the tilting or rotation of the holder of the polarising beam splitting prism (C2).

After one channel has been adjusted, the other one must be

checked. If a sine and cosine signal is put on to the oscilloscope and this is switched to XY operation, an ellipse is formed as shown in the following diagram.

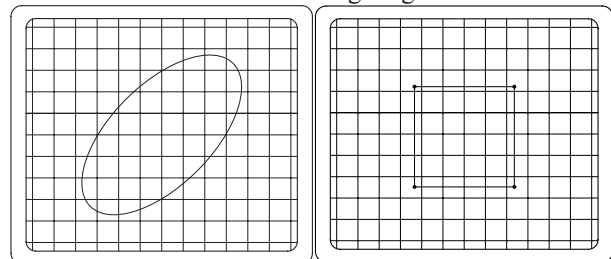
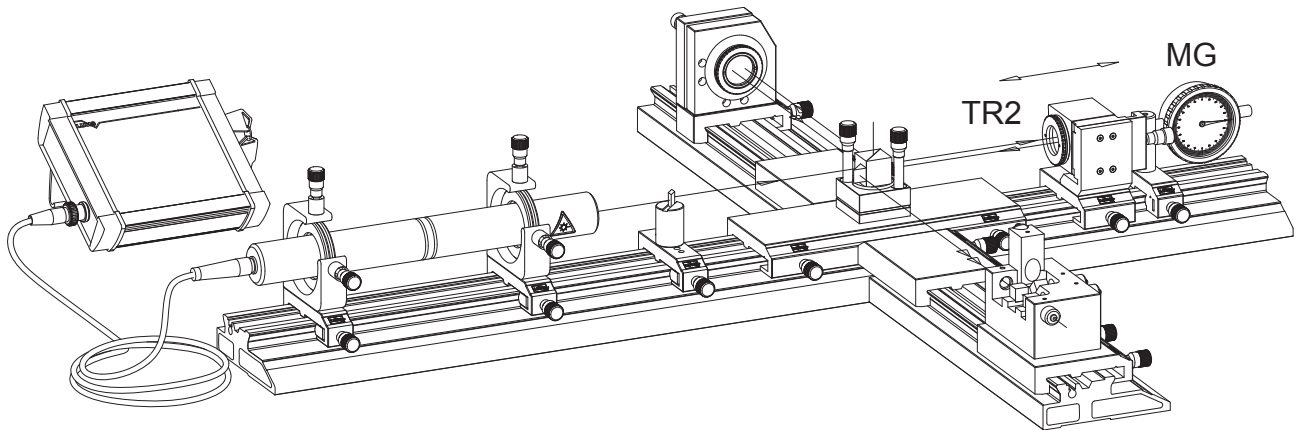


Fig. 71: Oscilloscope representation of the sine and cosine signal (left) and the TTL quadrature signals (right)

If the interferometer is at rest, then a point can be seen which moves either clockwise or counter clockwise within the ellipse, according to the direction of the movement. One round trip on the ellipse corresponds to a shift of $\lambda/2$. The principle of band interpolation can be explained at this point. The ellipse is transformed mathematically to a circle using a main axis transformation for this purpose. By finding out the position of the point (voltage X and voltage Y) the position of the interferometer can be given in fractions of λ . This is already 8.7 nm when a rough division is made at every 10° . If however, the TTL signals whose phases are shifted by 90° are displayed on the oscilloscope in XY operation the point jumps around on a square either clockwise or counter clockwise.

From Fig. 71 we can see that a round trip which corresponds to $\lambda/2$ has four defined points. This is electronically evaluated and we obtain a fourfold number of impulses and an increase in resolution from $\lambda/2$ to $\lambda/8 = 79$ nm!

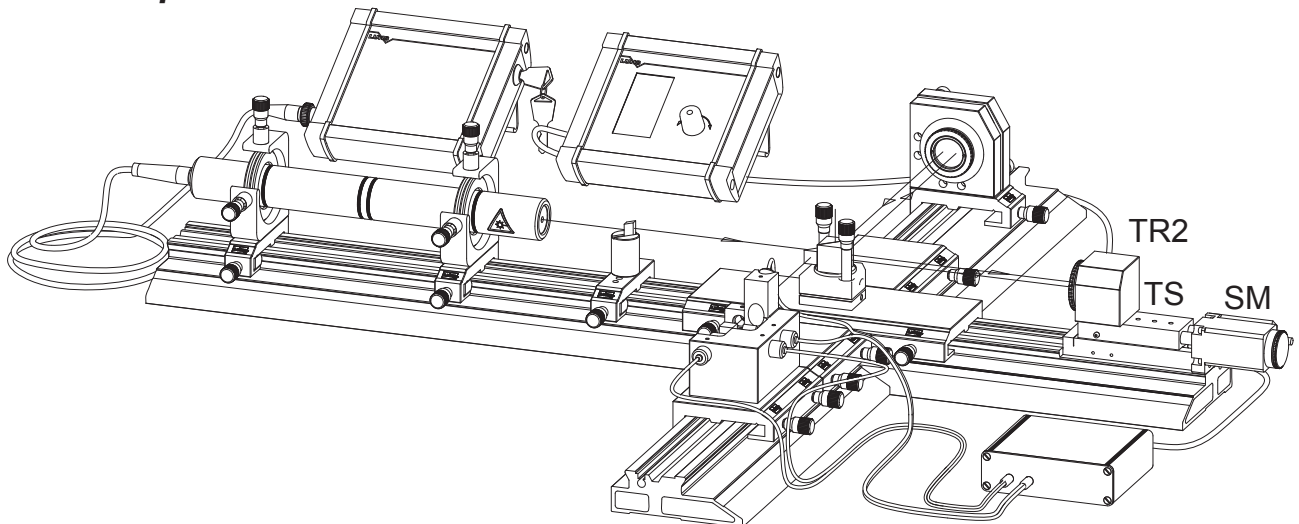
2.2.6 Length measurement



A micrometer dial gauge (MG), which is supplied with the set-up, will be used to measure the travelled path of reflector TR2. The gauge has an accuracy of 1 mm and a measurement range of 5 mm. The read-out of the gauge and the counter are compared whereby the laser interfer-

ometer forms the reference standard. For example each 0.5 mm travel indicated by the gauge the counter display is recorded. With this measurement the accuracy of the dial gauge can be verified and shows the principle of calibrating translation stages as used in modern CNC machines.

2.3 Set-up for CNC calibration



An elegant possibility for the display of the travelled path in mm or other suitable dimensions is the PC – counter card. This card fulfils the same purpose as the counter FC-01 but the count events can be stored and the further evaluation can be done by using software. Furthermore the manual driven stage of T2 can be replaced by a motorised version controlled by the software.

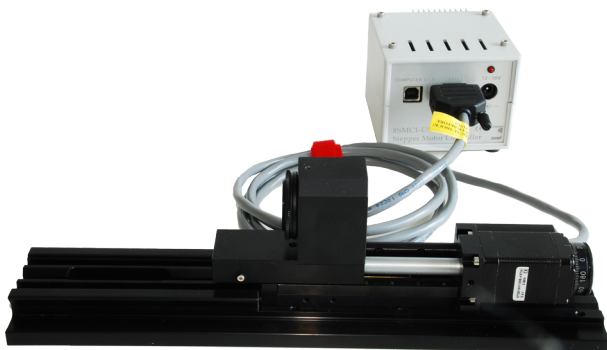
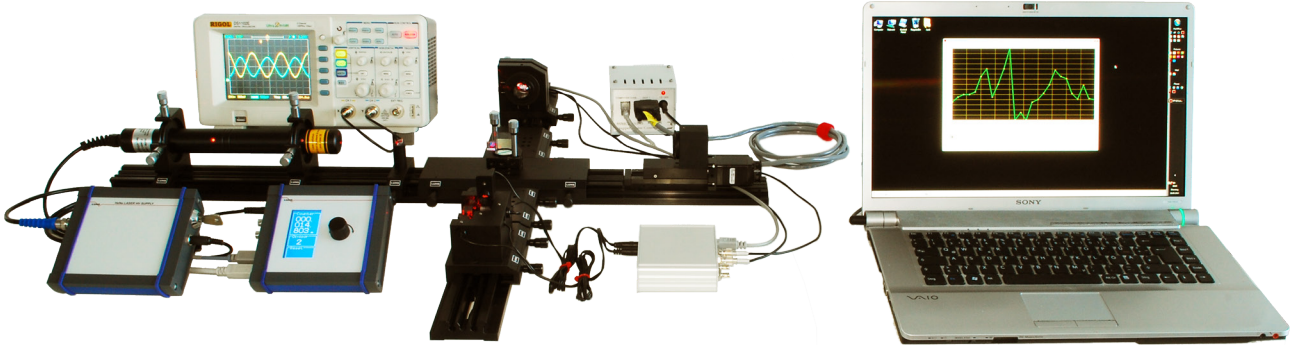


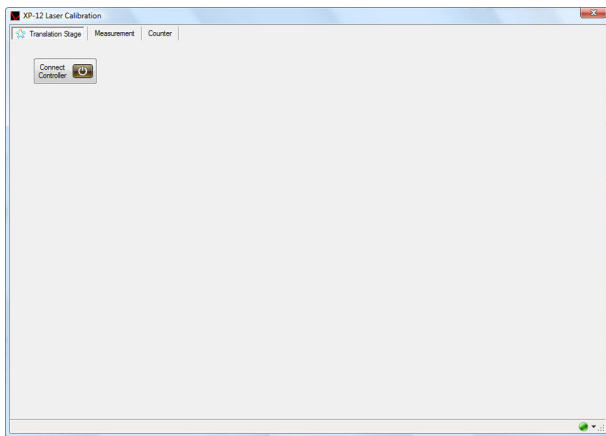
Fig. 72: Translation stage (TS) driven by a micro step motor (SM) carrying the triple reflector TR2

2.3.1 Set-up showing the use of a computer

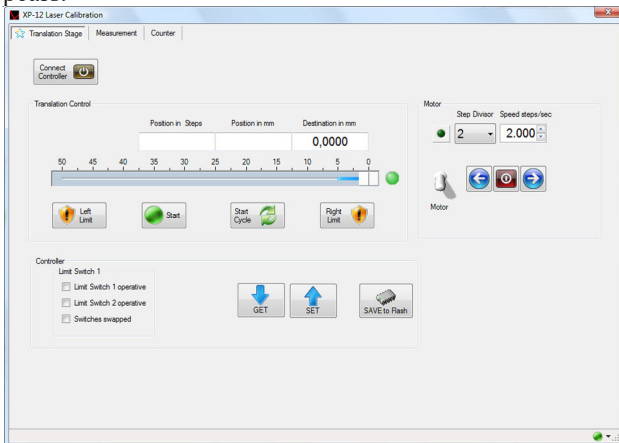


2.4 Calibration Software

Before the software can be used, the driver for the stepper motor controller needs to be installed. After the set-up and starting of the main software the following screen appears.



Click on the button to connect the controller to the computer. If the connection was successful the next screen appears.



Three sections are displayed. Within the translation control section the numerical controlled movement of the translation stage is set and monitored. To calibrate the translation stage, firstly the “Right Limit” button is pressed to let the translation stage move to the home position and set this position to zero. A destination can either be entered or selected by moving the glider of the slide control. For alignment purposes a cyclic movement can be obtained. The distance is chosen and by clicking the “Start Cycle” button the cycle is started. Clicking again the button the movement stops.

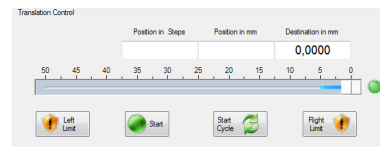


Fig. 73: Translation control section

Within the motor section the settings of the stepper motor are done. The motor can be switched on and off by clicking the switch. One step of the stepper motor can be divided by 2,4 and 8. The higher the divisor the smoother the movement will be.

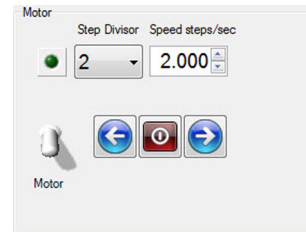


Fig. 74: Motor section

For testing purposes the motor can be started and stopped by clicking the respective buttons.

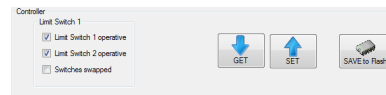


Fig. 75: Controller section

It is of importance that the limit switches are operative and are not swapped in their function. If not, set the options, click on “SET” and “SAVE to Flash”

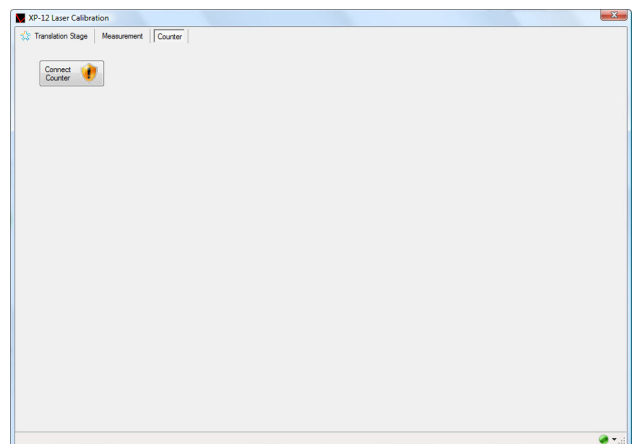


Fig. 76: Connect to counter

Set-up showing the use of a computer

Within the next step the software connects to the counter. For this purpose the button  is clicked.

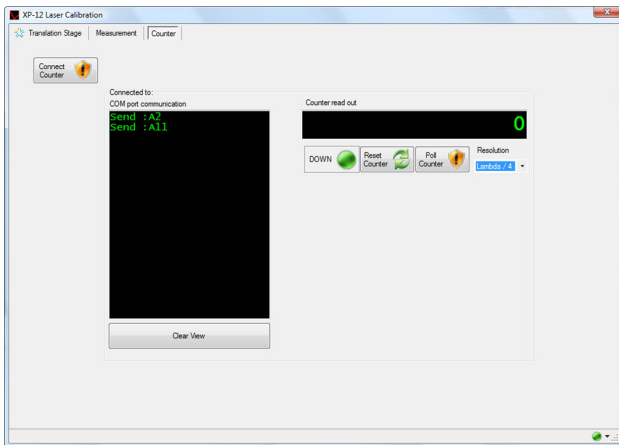


Fig. 77: Counter connection

Once the counter is connected the commands and response is displayed in The COM port communication window.

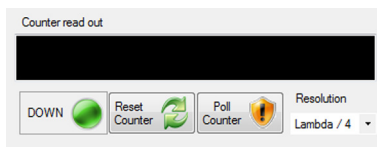


Fig. 78: COM port communication

By means of these controls the communication can be tested and the counter result displayed in the “Counter readout” field. The resolution of the counter can be set to $\lambda/2$, $\lambda/4$ or $\lambda/8$.

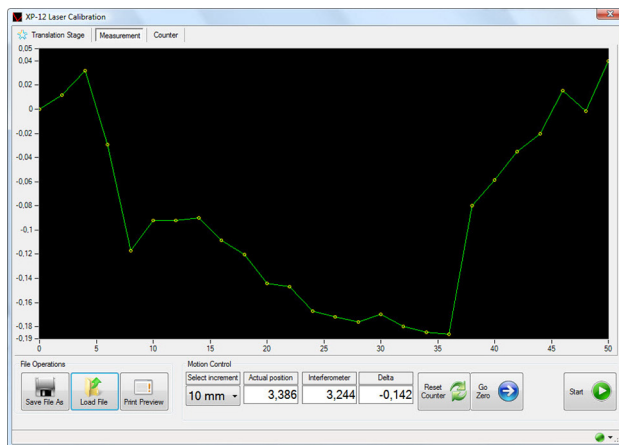


Fig. 79: Measurement display

Once the translation stage as well as the counter are operated properly, the automated measurement can be started. For this purpose the “Measurement” is activated.

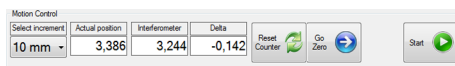


Fig. 80: Motion Control section

In this section the settings for the measurements are done. Firstly the translation stage must be moved to its zero position (GO Zero button). The counter will be reset by clicking the “Reset Counter” button. Before clicking the start button, the increment of travel should be selected. The translation stage will move by this value. During a short stop the counter read out is taken and the next increment

started until the stage reaches the maximum of 50 mm total travel. During the measurement the values are displayed. Once the measurement cycle is completed, the data can be stored or printed. In addition previously measurements can be loaded again.

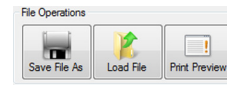


Fig. 81: File operation control